


REVIEW

Open Access



2D materials: increscent quantum flatland with immense potential for applications

Pranay Ranjan^{1*}, Snehraj Gaur², Himanshu Yadav², Ajay B. Urgunde², Vikas Singh², Avit Patel², Kusum Vishwakarma², Deepak Kalirawana², Ritu Gupta^{2*} and Prashant Kumar^{3*} 

Abstract

Quantum flatland i.e., the family of two dimensional (2D) quantum materials has become increscent and has already encompassed elemental atomic sheets (Xenes), 2D transition metal dichalcogenides (TMDCs), 2D metal nitrides/carbides/carbonitrides (MXenes), 2D metal oxides, 2D metal phosphides, 2D metal halides, 2D mixed oxides, etc. and still new members are being explored. Owing to the occurrence of various structural phases of each 2D material and each exhibiting a unique electronic structure; bestows distinct physical and chemical properties. In the early years, world record electronic mobility and fractional quantum Hall effect of graphene attracted attention. Thanks to excellent electronic mobility, and extreme sensitivity of their electronic structures towards the adjacent environment, 2D materials have been employed as various ultrafast precision sensors such as gas/fire/light/strain sensors and in trace-level molecular detectors and disease diagnosis. 2D materials, their doped versions, and their hetero layers and hybrids have been successfully employed in electronic/photonic/optoelectronic/spintronic and straintronic chips. In recent times, quantum behavior such as the existence of a superconducting phase in moiré hetero layers, the feasibility of hyperbolic photonic metamaterials, mechanical metamaterials with negative Poisson ratio, and potential usage in second/third harmonic generation and electromagnetic shields, etc. have raised the expectations further. High surface area, excellent young's moduli, and anchoring/coupling capability bolster hopes for their usage as nanofillers in polymers, glass, and soft metals. Even though lab-scale demonstrations have been showcased, large-scale applications such as solar cells, LEDs, flat panel displays, hybrid energy storage, catalysis (including water splitting and CO₂ reduction), etc. will catch up. While new members of the flatland family will be invented, new methods of large-scale synthesis of defect-free crystals will be explored and novel applications will emerge, it is expected. Achieving a high level of in-plane doping in 2D materials without adding defects is a challenge to work on. Development of understanding of inter-layer coupling and its effects on electron injection/excited state electron transfer at the 2D-2D interfaces will lead to future generation heterolayer devices and sensors.

Keywords: 2D materials, Synthesis, Characterization, Applications

*Correspondence: pranay.ranjan@iitj.ac.in; ritu@iitj.ac.in; Prashant.Kumar@newcastle.edu.au; magmemory@gmail.com

¹ Department of Metallurgical and Materials Engineering, Indian Institute of Technology Jodhpur, Karwar 342037, Rajasthan, India

² Advanced Materials and Devices Laboratory, Department of Chemistry, Indian Institute of Technology Jodhpur, Karwar 342037, Rajasthan, India

³ Global Innovative Centre for Advanced Nanomaterials (GICAN), College of Engineering, Science and Environment (CESE), School of Engineering, The University of Newcastle, University Drive, Callaghan, NSW 2308, Australia

1 Introduction to 2D materials

Pioneering breakthrough by Geim and Novosolev on micromechanical exfoliation to obtain sp² bonded atomic sheet of carbon i.e., *graphene* from naturally occurring layered material graphite in 2004 led to the 2010 Nobel prize in Physics [1]. Graphene on investigation exhibited a Dirac nature and the quantum Hall effect. Apart from the single-crystal nature at atomic thickness, several attributes such as high surface area, world record electronic mobility, excellent thermal conductivity, superior

Young's modulus, and chemical stability up to 300 °C were remarkable. Graphene has revolutionized materials science and engineering. Applications spanning over electronic chips, electron tunneling devices, LEDs, solar cells, energy sector, laser shields, light combat aircraft, night vision cameras, advanced electronic gadgets, SERS based molecular detection, gas sensing prompt disease (viral/cancer/diabetic) diagnosis [2–19], etc. have rendered it a wonder material. Moreover, Moiré-hetero layers of graphene have been amusing with interesting quantum behavior in terms of its unconventional superconducting and magnetic behavior. Quantum electronic signatures emerging out of graphene has established it as one of the best-known quantum materials and has opened up enormous possibilities [20]. Due to the lack of sufficient charge carriers, and zero bandgap, in graphene the ON/OFF ratio exhibited was found to be negligible, and this hampers its prospect as an ideal candidate active layer for electronic chips. To overcome these limitations, doping of graphene lattice [21–23] and its hybridization [24] with various two/three-dimensional materials have been devised. However, parallelly, new 2D materials such as elemental atomic sheets also called Xenes such as borophene, phosphorene, Stannene, Germanene, etc. were developed in the following years [25, 26]. Parallelly, boron nitride (BN) and TMDCs (e.g., Molybdenum disulfide, Tungsten disulfide) were developed [27]. Apart from TMDCs, 2D versions of metal oxides [28, 29] and metal phosphides [30] were discovered, while MXenes (Metal nitrides, metal carbides and carbonitrides, etc.) developed thereafter [31, 32]. A calendar of the 2D materials family is exhibited in Fig. 1. In this article, we elaborate on the evolution of the family of 2D materials, its synthesis protocols, and various technological applications. Challenges being faced by the quantum flatland have been elaborated. Furthermore, the scope and role of 2D materials in upcoming technologies have been presented.

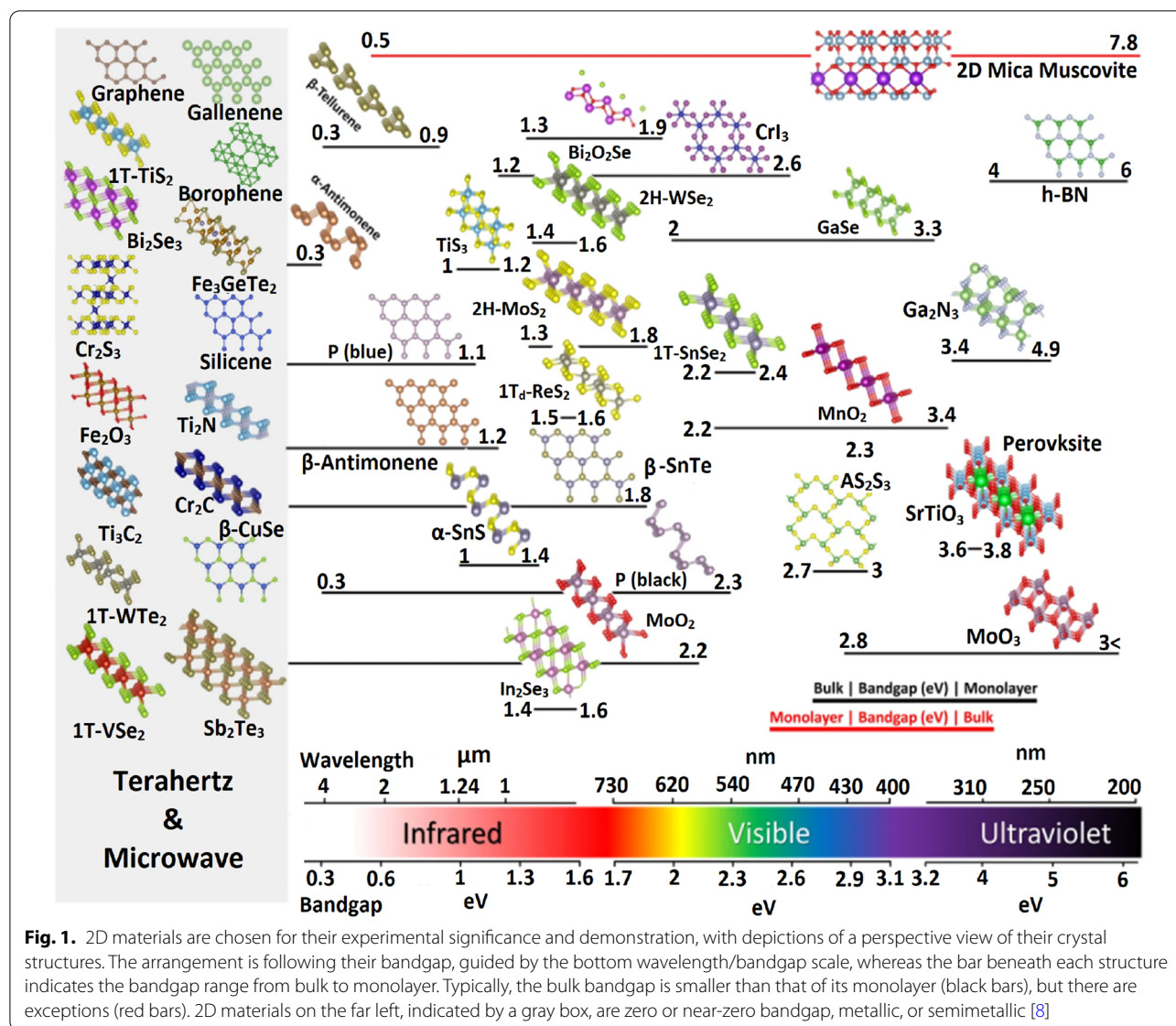
2 Synthesis of 2D materials

Synthesis methods for graphene include sonochemical exfoliation [2, 33, 34], arc discharge technique [35], Photo exfoliation [36, 37], Chemical vapor deposition [38], Laser chemical vapor deposition [39], Microwave plasma chemical vapor deposition [40] and unzipping of carbon nanotubes [41–43]. Chemical vapor deposition and arc discharge techniques are widely used for electronic devices due to their control over defect and thickness and thus helps in delivering the high-end product. However, these techniques are not suitable for industrial-scale due to the involvement of toxic gases, cumbersome deposition techniques, and the need for skilled labor at every stage of growth. The cost of the end product is

generally very high and thus limits the use of this technique to limited areas such as use in defense products, etc. To address the scalability issues, modified Hummer's method of oxidative exfoliation [44] followed by reduction has been employed widely by the scientific community. All these chemical-based intercalation methods are the fundamental techniques for large-scale production and involve interaction between solute and the material as well as an additional parameter such as the ultrasonic wave frequency/exothermic energy/photon energy or a blend of the two. The main advantage of using these techniques is that they can make 2D materials at a large scale at a low cost and don't involve the use of any toxic gases. However, these techniques involve certain issues like the inclusion of defects, functionalization, crumplings, wrinkles, fragmentation, and non-uniform sheet sizes and thus limit the use in electronic devices (particularly due to the opening of the bandgap). In addition, to remove the functionalities and end up with a clean pristine sheet different methodologies are being introduced. Among oxygen functionality reduction strategies, annealing in a hot air oven, microwave annealing [45], and laser reduction [46–48] are a few. Methods of synthesis for graphene have been widely adopted for the synthesis of other 2D materials too. For example, Ranjan et al. adopted micro-mechanical exfoliation and modified Hummer's method for the synthesis of borophene [49, 50] and micro-mechanical exfoliation. Sahu et al. [51] recently carried out a modified Hummer method of oxidative exfoliation of MoS₂ and BN [52]. Most of the synthesis techniques for graphene are material independent and can conveniently be employed for various Xenes and other 2D materials too. Methods of synthesis of 2D materials have been summarized in Fig. 2.

3 Characterization of 2D materials

Graphene, the atomic thin layer of carbon atom arranged in a hexagonal geometry contains sp² hybridized carbon atoms. It has sp²-hybridized planar bonds making 120° with each other, which gives the hexagonal arrangement of carbon atoms. Carbon has four valence electrons, out of which three electrons get hybridized in a sp² configuration (thus forming a bond), and the fourth electron forms the half-filled 2p_z, thus leading to the formation of π covalent bonds. This σ bond is considered to be the reason behind the unprecedented chemical and mechanical properties of graphene concerning other 2D materials. However, the electronic properties are related to the p-orbital that is always perpendicular to the lattice. The p-orbital usually leads to the formation of a covalent bond and forms the electronic π band. These half-filled bands result in exceptionally high electronic mobility or the carrier transport of graphene. Contrary to this the chemist



approach suggests that the key to enhanced electronic property of graphene lies in the orthogonality and non-interaction of the π and π^* states respectively. It has also been an area of debate that the linear dispersion observed in the graphene monolayer sheets is also due to the two orthogonal states. Thus, a chemical approach suggests that the structure and the nature of the bond (covalent) both lead to high mechanical strength and a higher value of the optical phonon frequency. These significantly high values of the phonon frequency (1600 cm^{-1}) in graphene as compared to the silicon ($\sim 520\text{ cm}^{-1}$), III–V compounds ($\sim 310\text{ cm}^{-1}$) lead to less optical phonon scattering than in comparison to the other existing conventional semiconductors. In addition, low scattering of the phonons and zero mass, as well as significantly high values of

the Fermi velocity carriers, induces ballistic regime and quantum tunneling which otherwise is not possible with other conventional semiconductors [1–4]. However, the experimentally observed values of the mobility in the graphene are much lower than the theoretically predicted values due to lattice defects, edge effect, ripples, crumples, or the presence of ad-atoms [4–12]. In addition, the electronic properties of the 2D materials further rely on the atomic number (electrons available), size of the atoms, chemical bonding, crystallography structure, and strain in the system.

The electronic mobility of the graphene sheets was reported to be $180,000\text{ cm}^2/\text{Vs}$, which is deemed to be the highest in comparison to atomic sheets of phosphorene, boron nitride, TMDCs, complex 2D materials such as

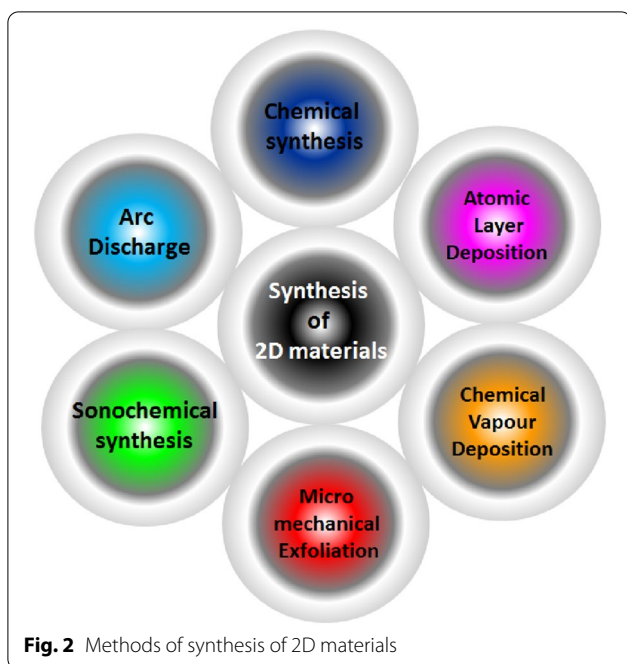


Fig. 2 Methods of synthesis of 2D materials

plumbene, hematene, etc. It would be worth mentioning that the 2D material family has gone far beyond graphene to mono-elemental sheets and complex 2D oxides (as shown in Fig. 3) and is now an extremely versatile system consists metallic, semi-metallic, semiconducting,

topological-insulators, and superconductors. Some of the cousins of graphene such as silicene, germanene, stannene, phosphorene, semiconducting molybdenum diselenide, tungsten diselenide, molybdenum disulfide, tungsten disulfide have mobilities such as 2100 cm²/Vs, 2800 cm²/Vs, 3000 cm²/Vs, 1000 cm²/Vs, 50 cm²/Vs, 180 cm²/Vs, 200 cm²/Vs, 0.2 cm²/Vs respectively (see Fig. 4).

Although these 2D materials have unique and unprecedented physical and chemical properties, they need to be synthesized in a pristine state and thus characterization techniques play the most important role in the investigation of these 2D materials' unique signatures. Among primary characterization techniques for 2D materials are microscopies (Optical, FESEM, AFM, and TEM/HRTEM) and spectroscopies (Raman, XPS, and FTIR). Most of the 2D materials have sharp characteristic Raman peaks. Graphene, for example, exhibits D, G, and 2D peaks at 1360 cm⁻¹, 1560 cm⁻¹, and ~ 3250 cm⁻¹ [53] with a typical I_{2D}/I_G ratio is the number of layer sensitive and is > 3 for monolayers if it is chemically pure. BN exhibits Raman peak at ~ 1360 cm⁻¹ [54]. MoS₂ exhibits E_{2g} and A_{1g} peaks at ~ 384 and ~ 403 cm⁻¹. Δ for the two Raman peaks for MoS₂ is layer dependent. Semiconducting 2D materials are characterized by their band gaps. Tauc plot obtained from UV-Vis's spectroscopy directly provides an estimate of the bandgap. The electronic bandgap can be obtained from R vs T measurement using the formula $R=R_0 \exp. (- E_g/k_B T)$. Hall effects have

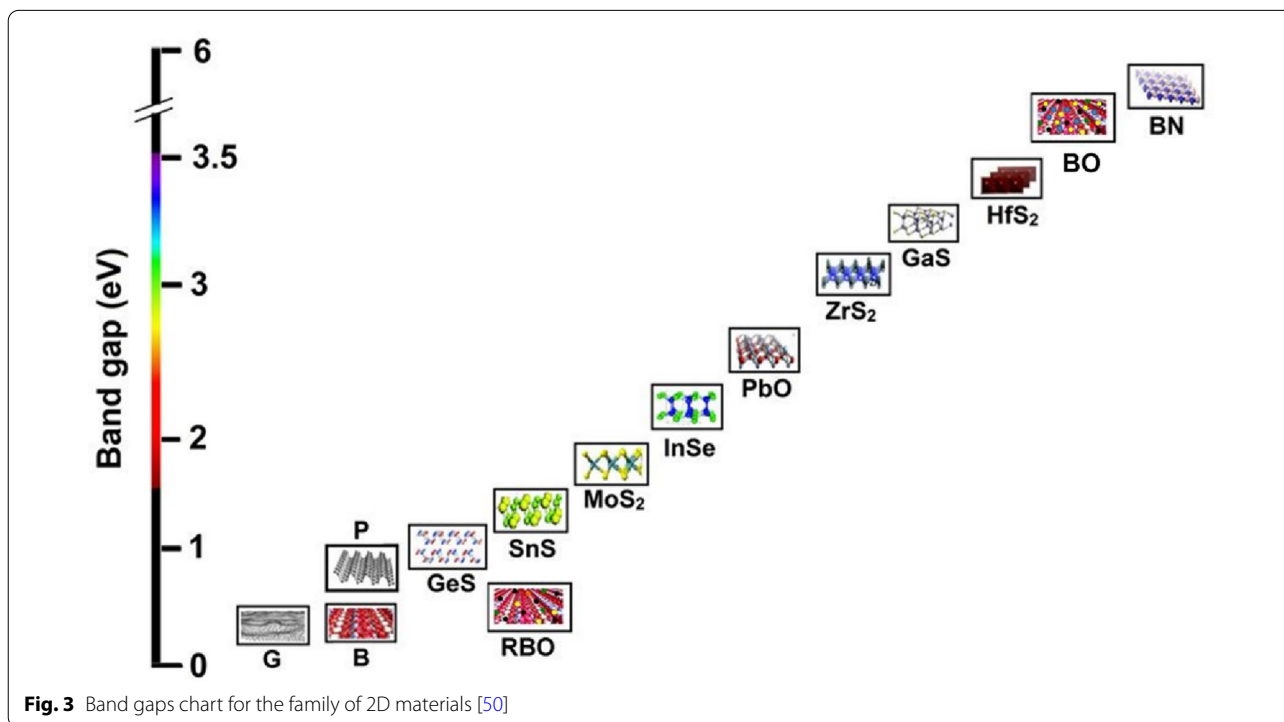
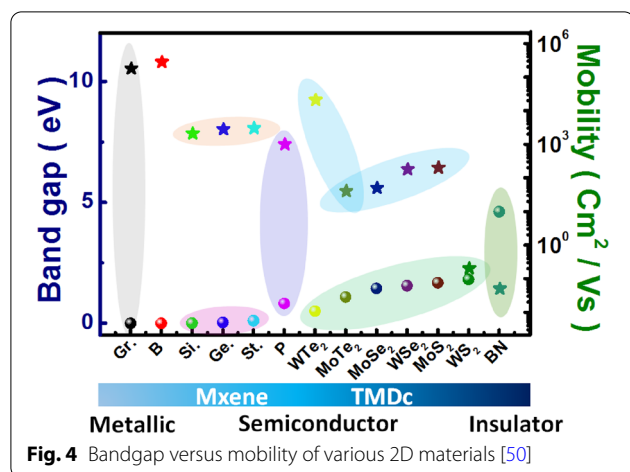


Fig. 3 Band gaps chart for the family of 2D materials [50]



widely been used for obtaining carrier concentration. Photoconductivity measurements provide information on applicability as active material in solar cells. Photoluminescence measurements are used to explore the feasibility of application for LEDs. FET device measurements yields electronic mobility and ON/OFF ratio to gauge the potential application in electronic chips. Nanomechanical testing has widely been used for evaluating young's moduli to explore mechanical applications. Electrochemical measurements provide a hint whether a particular 2D material is suitable for energy applications (battery and supercapacitor) or not.

4 Salient applications of 2D materials

4.1 Energy storage devices

The global rise in energy demands has paved the way for efficient energy storage devices. 2D materials with large specific surface area, high conductivity, and high electrochemical activity are promising for supercapacitors and batteries. The atomic-level thickness and high flexibility make them suitable for wearable energy storage applications [55]. Most conventional materials can't utilize their whole structure for electrolyte ion diffusion, hindering charge storage capability. Supercapacitors store energy in the form of an electric double layer or redox reaction at the electrode surface and thus require electrode materials with high specific surface area for enhanced device performance. Numerous 2D materials for supercapacitors include graphene, TMDs, and BP for higher conductivity, MXenes, Metal oxides, and layered double hydroxides for higher electrochemical redox activity while metal-organic frameworks and covalent organic frameworks with high surface area [56, 57]. Pristine 2D materials are not adequate for direct supercapacitor fabrication due to poor structural and chemical stability in the

electrochemical process, inert surface, lower electrical conductivity, and lack of active surface sites [58]. Various strategies have been adopted to address these issues by modifying the 2D materials through surface defects engineering, heteroatom doping, surface functionalization, and increasing interlayer spacing by intercalation and hybrid structures. MXene-based materials are used in high-performance supercapacitors due to their high conductivity, intercalation of polar organic molecules and metal ions, and facile adsorption of ions due to surface functional groups ($-O$, $-OH$, $-F$) [59]. Xia et al. demonstrated the capacitive performance of vertically aligned $Ti_3C_2T_x$ MXene films by mechanical shearing. The vertical alignment of MXene sheets led to facile ion transport, and the capacitance was retained up to 200 Fg^{-1} at 2000 mVs^{-1} (independent of the thickness of the film) [60]. Zhao et al. prepared sandwich and micro-sized supercapacitor electrodes using synchronous reduction and self-assembly of MXene on Zn foil. Due to the high electrical conductivity porous architecture, the devices showed excellent electrochemical performance even in bending states, demonstrating the application of MXenes for flexible and wearable energy sources [61]. 2D Transition Metal Oxides (TMOs) are another exciting class of electrode materials with high specific capacitance and energy density due to reversible redox reactions [62]. Some of the widely used metal oxides for supercapacitor electrodes include MnO_2 , $NiCo_2O_4$, RuO_2 , Fe_3O_4 , and NiO . Though metal oxides have a high specific capacitance of $200\text{--}2000 \text{ Fg}^{-1}$, they suffer from poor electrical conductivity, cracking of electrodes during cycling, and limited access due to varied coordination. Ma et al. investigated the performance of MnO_x nanosheets on $MnO_x@Carbon$ nanowire synthesized by liquid phase method with thermal treatment [63]. MnO_x nanosheets offer abundant surface-active sites for electrochemical activity. The all-solid-state supercapacitor fabricated using nanosheets of MnO_x show a maximum power density of 2500 W kg^{-1} and energy density of 23 Wh kg^{-1} with 94% capacitance retention up to 2000 cycles [63]. The effect of defect engineering on 2D materials was explored by Chen et al. using amorphous Vanadium Oxide nanosheets for asymmetric supercapacitors. The defects increased the oxygen vacancy content to 28.5%, facilitating ion migration and leading to the ultra-high specific capacitance of 554 mF cm^{-1} at 1 mA cm^{-2} [64]. Santos et al. reported a cost-effective, single-step synthesis of transition metal oxide (Co and Cu) grafted carbon nitride nanosheets. The asymmetric supercapacitor fabricated using Co and Cu oxides hybrid exhibited a specific capacitance of 124.5 F g^{-1} and 84.28 F g^{-1} with cycling stability of 96% retention after 2000 cycles [65]. Transition metal dichalcogenides (TMDs) finds application in supercapacitor due to their

large surface area and rapid redox reactions at the surface but possess low capacitance retention. Some of the widely used TMDs include MoS_2 , WS_2 , TiS_2 , NbS_2 , and VS_2 . In Fig. 5a, Adhikari et al. reported WS_2 -PANI composite, which exhibited excellent high-frequency supercapacitor. WS_2 -PANI composite exhibited the capacitance of 72.27 Fg^{-1} at 1 Ag^{-1} and a high-frequency response of 6 kHz . The device exhibits cyclic stability of 85% and coulombic efficiency of $\sim 100\%$ in Fig. 5b [66]. Some other novel 2D materials such as phosphorene, silicon, bismuth and, stannene, have been explored for supercapacitor application due to their properties analogous to graphene. [67] Kim et al. performed the first polymerization of 2D Phosphorene using conducting

polypyrrole. The specific capacitance of hybrid was reported to be 411 Fg^{-1} which is four times as compared to polypyrrole as electrode material [68]. Phosphorene is a good is electrode materials that are highly hygroscopic and sensitive to ambient atmosphere. In addition, various transition metal oxides and carbon-based are used as electrode materials but they lack due to poor conductivity and low density, respectively. It been observed that the 2D layered materials with sheets arranged in specific manner in crystals are best since it offers high surface exposure for reaction as compared to other conventional electrode material [69]. Graphene, porous carbon sheets, and carbon nanotube are well reported for their supercapacitive application and commercialization. Graphene is

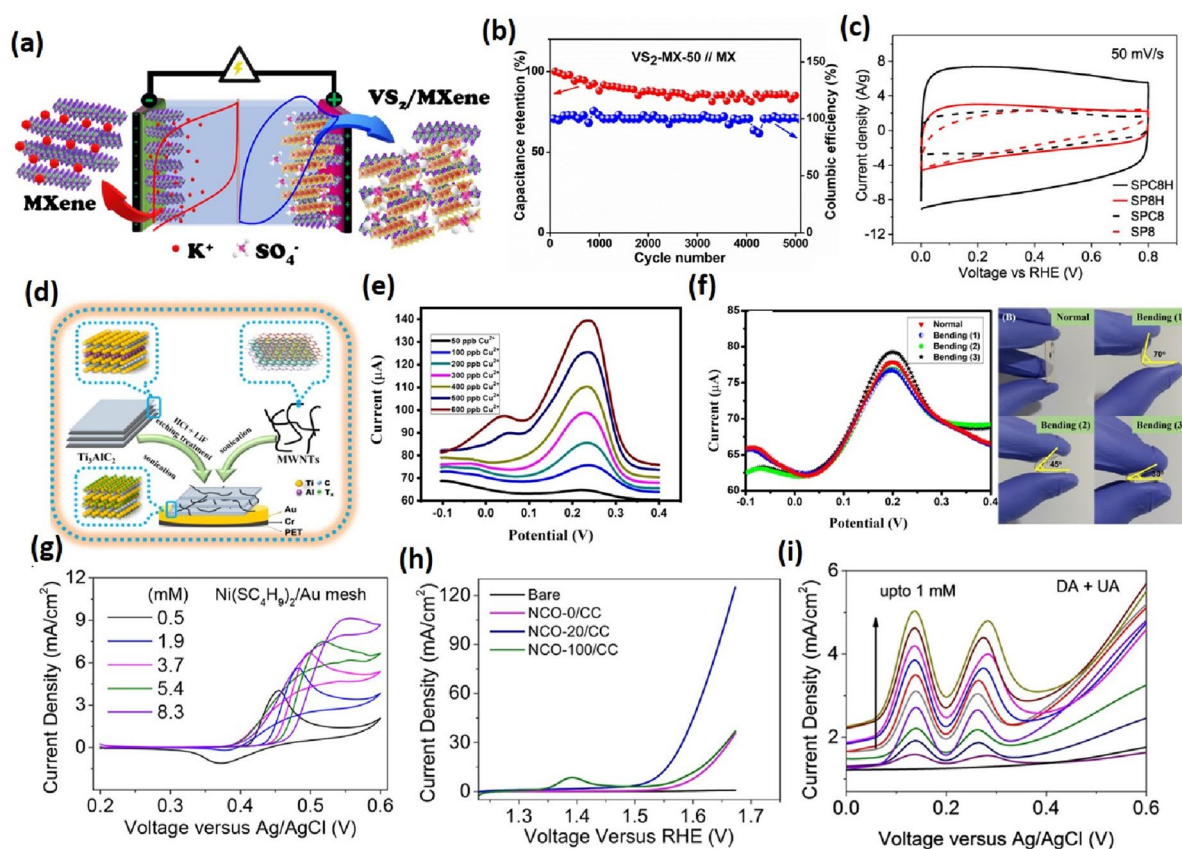


Fig. 5 **a** Schematic representation of charge transfer and storage mechanism of the VS_2 -MX-50//MXene asymmetric device **b** Cyclic Stability (85%) and Coulombic Efficiency ($\sim 100\%$) of the VS_2 -MX-50//MX asymmetric device at a current density of 30 A/g . Figure adapted from reference [66] **c** Cyclic Voltammograms at a scan rate of 50 mV/s in the graphitic carbon electrodes. Figure adapted from reference [76] **d** Modification process of the flexible $\text{Ti}_3\text{C}_2\text{Tx}/\text{MWNTs}/\text{Au}/\text{PET}$ working electrode. **e** SWASV responses of the $\text{Ti}_3\text{C}_2\text{Tx}/\text{MWNTs}/\text{Au}/\text{PET}$ electrode for the determination of Cu(II) with various high/MW concentrations in ABS (0.1 M , $\text{pH } 4.6$): $50 - 600 \text{ ppb}$. **f** SWASV responses of the $\text{Ti}_3\text{C}_2\text{Tx}/\text{MWNTs}/\text{Au}/\text{PET}$ electrode for the determination of 300 ppb Cu(II) in normal and different bending states and display of different bending processes of the fabricated electrode. Figure adapted from ref. [84] **g** Cyclic Voltammogram of $\text{Ni-C}_4\text{SH}/\text{Au}$ mesh as working electrodes in the glucose of different concentrations at a scan rate of 50 mV s^{-1} Figure adapted from ref [85] **h** LSV curves at 5 mV/s of Ni-Co oxide nanoplate Figure adapted from ref. [86] **i** Simultaneous measurements with increasing concentration of equimolar Dopamine and Uric Acid from 1 nM to $1000 \text{ }\mu\text{M}$, respectively (Figure adapted from ref [87])

2D layered material with excellent mechanical strength, high surface area, and, high conductivity due to sp^2 hybridized carbons in 2D sheets structure. Despite this, graphene nanosheets undergo restacking decreasing electrolyte charge distribution at the electrode surface. To overcome this issue, chemical functionalization of graphene/graphene oxide with heteroatoms, intercalation, etc. has been done for better supercapacitive performance [69, 70]. Robert A. W. Dryfe and coworkers prepared N-doped graphene oxide with hexamethylenetetramine by the hydrothermal process followed by thermal expansion resulting in a high specific capacitance value of 270 F/g at 1 A/g [71]. Park et al. used 2D controlled oxidized black phosphorous covalently bonded to graphene and achieved a high capacitance value of 478 F/g [72]. To fulfill the modern need for flexible and portable energy devices, flexible supercapacitors are developed. Yan Li and their group made a flexible solid supercapacitor by coating gel electrolyte and N-doped CNT/GO composite to both sides of the paper. A high volumetric capacitance value of 0.45 F/cm^3 was reported and an energy density of $40.0 \mu\text{Wh/cm}^3$ [73]. Zheng and coworkers prepared a 2D hierarchical porous carbon nanosheet using polyaniline with acetaldehyde followed by carbonization and activation by KOH and achieved a volumetric capacitance of 3.8 F/cm^3 with a high energy density of 8.4 mWh/cm^3 [74]. Chong et al. synthesized MoS_2 /graphene composite by electrochemical etching of bulk MoS_2 and graphite electrode to prevent restacking of MoS_2 for supercapacitor with a high specific capacitance of 227 F/g and capacitance retention up to 89% over 2500 cycles [75]. Gupta and co-workers developed a catalytic approach to convert waste polystyrene into highly conducting graphitic carbon sheets with high surface area for electric double-layer supercapacitors with a high specific capacitance of 158 Fg^{-1} , linear response with scan rate, and 90% capacitance retention after 10,000 cycles. [76] Gordon G. Wallace and the group synthesized MoS_2 /PEDOT: PSS (MP) hydrogel by the one-pot hydrothermal process by controlling the growth of MoS_2 on the PEDOT surface. The supercapacitor device with solid-state electrolyte $\text{PVA-H}_3\text{PO}_4$ resulted in a high capacitance of 360 mF cm^{-2} at 0.5 mA cm^{-2} with capacitance retention of 89% [77]. Li et al. prepared a composite of oxygen vacancy-rich NiCoO_4 with nitrogen-deficient graphitic carbon nitride by one-pot heat treatment in presence of air. The high specific capacitance of 1998 F g^{-1} at a current density of 2 A g^{-1} was achieved with 95.22% capacitive retention after 5000 cycles [78]. Nayak and group synthesized a composite of SnS_2 with oxygen functionalized graphitic carbon nitride and CNT by a hydrothermal process resulting in a high specific capacitance of 433 F/g and 101% capacitance

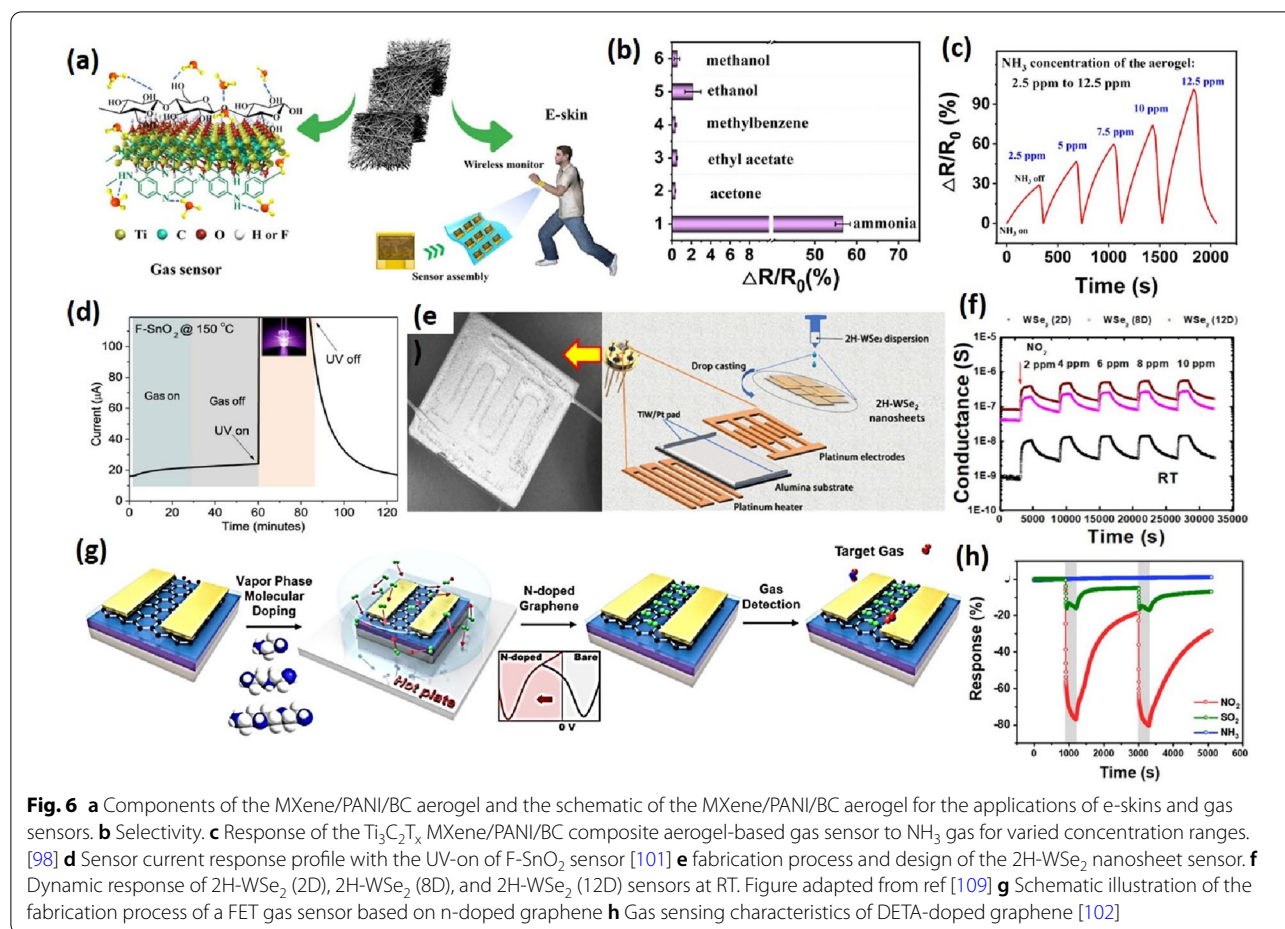
retention over 7000 cycles [79]. Sundramoorthy and group synthesized free-standing flexible electrode with a composite of hexagonal boron nitride and graphene paper by vacuum filtration of a mixture of h-BN and graphene nanosheets dispersions achieving excellent specific capacitance of 321.95 F/g at a current density of 0.5 A/g with 96.3% capacitance retention after 6000 cycles [80]. Dai and his group prepared alternative stacked 2D/2D MXene/ZnMnNi layered double hydroxides through electrostatic self-assembly of negatively charged MXene surface and positively charged ZnMnNi LDH surface by a simple string of their water dispersions, which showed capacitance value of 2065 F/g at a scan rate of 5 mV/s and with capacitance retention of 99.8% after 100,000 cycles at a current density of 1 A/g [81]. NPs were also used as an interlayer spacer for pseudocapacitive performance. For example, Warsi and coworkers intercalated CoFe_2O_4 NPs to prepare CoFe_2O_4 /MXene composite providing much higher capacitance (1268 F/g) and 97% capacitance retention up to 5000 cycles [82]. Rout et al. synthesized a composite of 1 T phase of VS_2 nano-flower with 2D MXene by in-situ hydrothermal method to achieve a high specific capacitance value of 115.7 F/g at a current density of 0.8 A/g with 85% capacitance retention over 5000 cycles, as well as the highest energy density achieved was 41.13 W h/kg [83].

4.2 2D materials for Gas/VOC and humidity sensors

Development in industrialization has led to a rapid rise in air pollution due to toxic gases, smoke, and emission, which pose a serious threat to human health. Various indoor air pollutants in volatile organic compounds (VOCs) come from paints, cosmetics, furnishing, glues and adhesives, cleaning and disinfecting products, etc. Exposure to toxic gases/VOCs higher than the maximum permissible limit or prolonged exposure causes severe health problems. Thus, gas and VOC sensors that can detect and monitor toxic gases in the environment have become extremely important for environmental monitoring. They are also a potential candidate for healthcare applications for detecting various biomarkers for disease diagnosis. The concentration of VOCs in human breath act as biomarkers for different disease such as toluene for lung cancer, acetone for diabetes, ammonia for renal failure, nitric oxide for asthma, etc. However, detecting the gas/VOCs at ppb level in a varying humidity atmosphere is extremely challenging. There is a dire need to develop sensing materials that are highly specific and sensitive toward selective molecules even under humid conditions [88]. For real-time monitoring and industrial application, the gas sensors need to be highly responsive, selective, have low fabrication cost, and have low power consumption. 2D materials have proven highly efficient due to

their fascinating chemical and physical characteristics. Prospects for 2D materials include stability of the material in an ambient atmosphere with room-temperature operation for practical application. A diverse range of 2D materials has been explored for gas sensing, including carbon nanomaterials, layered metal oxides, transition metal dichalcogenides, conducting polymers, MXenes, Borophene, carbon-based 2D materials, etc. [89]. These materials have advantages and disadvantages, such as high operating temperature, low conductivity, and low surface area. 2D materials, due to their unique physical and chemical property, mechanical flexibility, and high electron mobility, are widely used for gas sensing applications [88, 89]. The gas-sensing performance depends on various parameters such as sensitivity, selectivity, stability response/recovery time, detection limit, reproducibility, and reversibility. 2D layered materials offer high specific surface area and tremendous reactive adsorption sites leading to high sensitivity due to facile analyte-material interaction. Moreover, higher conductivity leads to low noise and results in relatively lower Limits of Detection. Owing to tunable surface functionalization in 2D material, they provide high selectivity by tuning the surface in a way to provides strong affinity towards the target gas. As the surface of 2D materials is highly sensitive, even a small change in the physical parameter of sensing material will lead to a detectable signal and hence provide good reversibility [90]. A large surface-to-volume ratio and tunable surface endow 2D materials with excellent properties for sensing application. Tailoring the morphology and surface structure by novel metal ion doping or heterostructure formation can significantly improve the sensing performance [91]. When 2D materials with different electrical properties come in contact, they form heterojunction at the boundary by carrier diffusion and Fermi-level alignment. The depletion layer formed at the junction has high resistance, changing when interacting with the gaseous analyte. The heterostructure of 2D materials includes metal–semiconductor which gives rise to the Schottky barrier or semiconductor–semiconductor junction (p-p, p-n, and n-n heterojunction) [91]. The gas-sensing performance can be improved by making 2D heterostructures with 0D, 1D, 2D, and 2D nanomaterials. Moreover, several heterostructures have been reported in the literature for enhanced sensing performance, but which electronic and chemical effect leads to which type of sense has not been fully explored and explained yet. Therefore there is a need to develop an insight into the typical chemical and electronic changes caused by the type of heterostructures for predicting the sensor behavior towards a specific analyte [91]. Among all layered materials, 2D Transition Metal Oxides (TMOs) are most extensively being utilized for sensing applications due to

reduced bonding coordination and high surface polarization with fascinating chemical and physical properties than their bulk counterparts. Metal Oxides have pre-adsorbed oxygen on the surface which leads to the formation of an electron depletion layer on the surface. When an analyte interacts with the surface, depending on the nature of the interacting analyte it will either increase or decrease the thickness of the depletion region and hence change the resistance of the material. Metal oxides nanosheets have a large specific surface area and thickness equal to Debye length. They have strong in-plane bonds and weak van der Waals interaction between layers [92]. The adsorption of a gas on metal oxide act as either p-type or n-type dopants depending on oxidizing or reducing nature of the gas, leading to a change in carrier concentration and hence changing the conductivity of the material. Metal Oxides work in an aerobic environment at high temperatures. Some commonly used 2D metal oxides for gas sensing applications include SnO_2 , WO_3 , MoO_3 , TiO_2 , and their composites. Despite various advantages of metal oxides for gas sensing, they suffer from high operating temperature, which can be addressed by using 2D materials with heterostructures. Wang et al. fabricated a sensor using Graphene oxide/ SnO_2 nanosheets with a response as high as 2000 towards HCHO. The excellent performance of the sensor was due to the synergistic effect of the sensitizer effect of GO, ultrathin nanostructure, and in-plane mesopores which are conducive to gas diffusion [93]. Qin et al. synthesized Co-based bimetallic metal oxide nanosheets for CO sensing. The sheets possess an ultra-high surface area of $220.7 \text{ m}^2 \text{ g}^{-1}$, exposing abundant active sites. The sensor exhibited ppb level detection with room-temperature operation [94]. Jang et al. developed subatomic level thick heterogeneous oxide $\text{SnO}_2/\text{CoO}_x$ nanosheets for gas sensing. The heterogeneous oxide was synthesized using an exfoliation approach and a Galvanic replacement reaction. The GRR process leads to the formation of plentiful $\text{SnO}_2/\text{CoO}_x$ heterojunction with high porosity and sub-10 nm thickness which are highly desirable for gas sensors. The sensor also showed exceptional selectivity towards formaldehyde gas at 5 ppm with recovery in $<10 \text{ s}$. The synthesis procedure adopted also opens ways for scalable production of heterogeneous oxides for sensing applications [95]. Various MXene-based hybrid materials have been reported in the literature for sensor fabrication for different gas/VOCs. Sun et al. reported a susceptible and selective NO_x sensor using $\text{Co}_3\text{O}_4@\text{PEI}/\text{Ti}_3\text{C}_2\text{T}_x$ nanocomposite with a low limit of detection of 30 ppb at RT. The heterojunction between p-type Co_3O_4 and conducting MXene provides facile electron transport for NO_2 sensing [96]. In Fig. 6a–c, Zhei et al. demonstrated a flexible pressure and gas sensor using MXene/



PANI/ bacterial cellulose aerogel with high selectivity toward NH_3 . The 3D structure improved the synergetic effect and enhanced the electron transfer due to improved gas adsorption and diffusion. The H-bonding between MXene, PANI, and BC provided stability to channels. The LOD value was determined to be 56.49 ppb [97]. Kim et al. reported a self-assembly method to intercalate metal ions in MXene forming transparent films that were utilized as gas sensors to detect ammonia. The intercalation improved the signal-to-noise ratio to tenfold compared to pristine MXene. The sensing performance of Na, K, Mg, and Ca intercalated MXene was compared, out of which Na-MXene showed the highest response with LOD of 10 ppm due to low film thickness and high electrical resistance [98]. He et al. developed a gas sensor based on MXene/SnO₂ heterojunction for ammonia sensing at RT. The difference in Fermi level of SnO₂ and MXene enhanced the sensitivity by facile charge transfer at the interface. The sensor showed excellent sensitivity from 0.5 ppm to 100 ppm ammonia with a 20 times higher response to 100 ppm ammonia [99]. Liu et al. fabricated a gas sensor using α -Fe₂O₃ nanocubes/

$Ti_3C_2T_x$ composite with excellent selectivity towards acetone. The α -Fe₂O₃ nanocubes attached to the MXene sheets by electrostatic interaction provided a higher active surface area for gas adsorption. The sensor showed linear response from 5 to 200 ppm acetone concentration with rapid response and recovery time of 5 s [100]. In Fig. 6d, Bahuguna et al. fabricated a thin-film F-SnO₂-based sensor for VOC detection [101]. In Fig. 6g, h Kwon et al. reported an N-Channel graphene sensor for NO₂ detection with a detection limit as low as 0.83 ppm [102]. Borophene, with its high electronic conductivity and large surface area, finds application in gas sensing [103]. Hou et al. reported the first NO₂ gas sensor based on borophene with high sensitivity, fast response, high selectivity, and good stability. The sensor also showed good stability for up to 1000 bending cycles, making it suitable for wearable electronics. Although borophene-based sensor shows a strong response to NO₂ the sensitivity is still lower than carbon nanomaterials and polymer composites [104]. Another research, conducted by the same group, demonstrated the graphene-borophene heterostructure for humidity sensing. The sensor showed

ultrahigh sensitivity, almost 700 times higher than graphene. The sensitivity towards humidity was as high as 4200% at 85% RH, the highest among all 2D materials [105]. Shen et al. theoretically investigated the adsorption behavior of organic molecules CH_4 , C_2H_4 , C_2H_2 , CH_3OH , and HCHO on Borophene and borophene/ MoS_2 heterostructure. C_2H_2 and HCHO show strong interaction with borophene and the heterostructure shows high sensitivity towards these molecules [106]. Various computational studies reveal that Borophene is an emerging class of 2D nanomaterials and has much potential for gas sensing applications, but experimental research is still very limited. For gas/VOC sensing, the performance of Transition Metal Dichalcogenides (TMDs) surface structure modifications, defect engineering, exposed edge sites, and doping have been explored. Pham et al. fabricated a MoS_2 -based optoelectronic NO_2 sensor using graphene. The sensing performance was enhanced by inducing photocurrent. The sensor showed high sensitivity and low limit of detection upto 0.1 ppb. TMDs-based gas sensors have sluggish recovery and have cross-sensitivity towards multiple analytes [107]. Ko et al. worked on enhancing of recovery performance of WSe_2 -based gas sensors. The sensor showed excellent sensing performance towards NO_2 with a response value of 4140%. The recovery was improved by using external thermal energy and by reacting NH_3 with adsorbed NO_2 on the surface which decreased the recovery time from 85 min to 43 s [108].

4.3 Electrochemical sensors

Modern chemical sensors use various features to determine biological, physical, and chemical aspects in day-to-day life [110]. Some examples are health sensors, environmental monitoring, sensors for instrumentation, and sensors related to machineries like airplanes, automobiles, and mobile phones [111]. Electrochemical sensors measure the electrochemical reactions and determine them with the help of electrodes due to the analyte and the sensing surface interactions, converting the information into quantitative and qualitative electric signals based on potentiometry, conductometry, and amperometry measurements [112]. The signal is measured by detecting changes in the faradaic current or interfacial resistances. The mechanism involves the usage of redox mediators to determine the capturing of a specifically targeted molecule onto the working electrode. The redox mediator accessible surface area decreases as the target analyte is captured, resulting in a drop in electrochemical current or a rise in interface resistance [113]. The development of novel 2D nanomaterials for working electrodes is crucial in advancing electrochemical sensors. Two-dimensional layered materials exhibit a high value of surface-area-to-volume ratios for analyte

interaction and a very high environmental sensitivity, which are important for chemical sensing applications [114]. Furthermore, 2D-nanomaterials possess excellent resilience and flexibility, making them capable of developing a new class of high-performance flexible electrochemical sensors [115]. By facilitating the electron transfer process and signal creation, 2D layered materials in electrochemical sensor devices seek to improve sensitivity and performance. Electrochemical sensors have the potential to determine analytes at much less concentration than state-of-the-art sensing technologies [116]. For example, Rahman et al. fabricated a sensing platform based on graphene oxide and silver nanowire nanocomposite for improved sensing performance of Hg^{2+} [117]. Choi et al. fabricated a graphene oxide doped diamino-terthiophene-based sensor to simultaneously determine copper, cadmium, mercury, and lead at a very low concentration [118]. Different chemical sensors have been developed based on 2D materials for various analytes that must be monitored, such as toxic metal ions, pesticides, herbicides, soil, and other important pharmaceutical compounds, bio-molecules like glucose, dopamine, uric acid, and cholesterol [119, 120]. For example, Murugan et al. developed an electrochemical sensor to simultaneously detect uric acid, dopamine, and ascorbic acid. The detection limit was 0.06 μM , 4.6 μM , and 0.075 μM for dopamine, ascorbic acid, and uric acid, respectively [121]. Ribeiro et al. fabricated an enzyme-free electrochemical sensor using an rGO and cobalt oxide hybrid material recycled from Li-ion batteries to determine ascorbic acid [122]. Also, conventional materials are used for the nonenzymatic-based determination of glucose; however, it is still challenging to detect it at a neutral pH. Many of the previous reports for the detection of glucose use highly alkaline solutions, which are difficult to implement for continuous monitoring and wearable systems. By incorporating 2D materials and improving the sensitivity, sensors for glucose determination in the neutral electrolyte have been developed. For example, Chen et al. reported a glucose sensor based on a nonenzymatic method at a neutral pH using graphene nanosheets modified with Pt–Pd nanocubes covered electrode [123]. In Fig. 6e, f, Moumen et al. fabricated a NO_2 sensor with a 2H variant of tungsten diselenide with a 361% response to 6 ppm NO_2 [55]. Foroughi et al. developed graphene-modified CuO nanoparticles for glucose sensing at biological pH [124]. Hybrids of 2D layered materials and their heterostructures utilize transition metal redox centers for interaction with the analytes and fabrication of multiplexed sensing systems. Reactive nitrogen species (NS) and Oxygen species (OS), such as NO or H_2O_2 , are important molecules involved in cellular metabolism and several signaling processes inside the body [125]. A

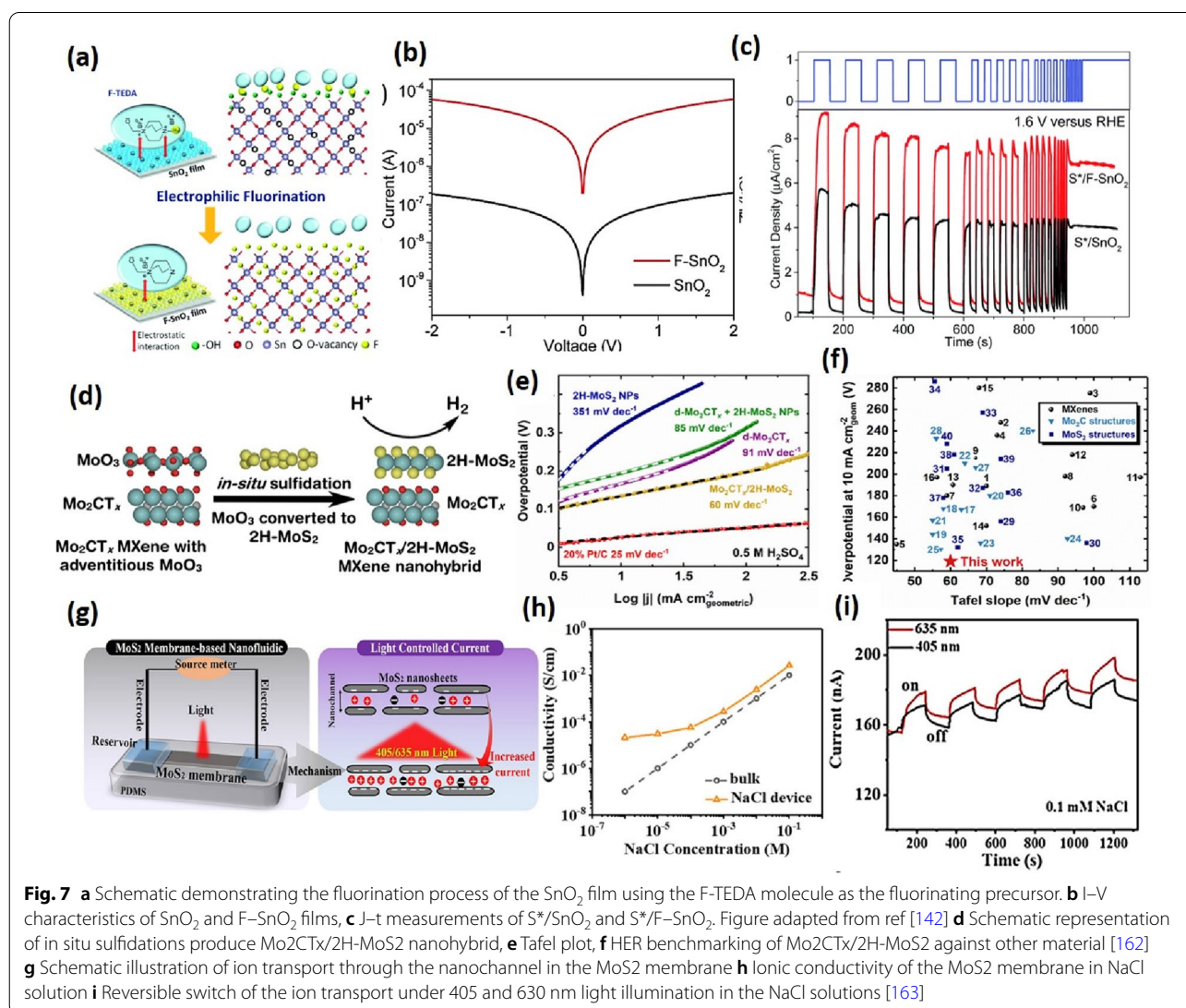
nitrosative and oxidative stress can occur if the concentrations of NS/RO are left unbalanced by the antioxidant system in the body, and long-term stress can cause various diseases such as Alzheimer's, Parkinson's, and cancer [126, 127]. Therefore, proper continuous monitoring of their concentrations becomes important for identifying disease and good health. Electrochemical detection of heavy metal ions (HMIs) at ppm and ppb levels depends on the electrochemical reactions occurring due to metal ions at the interface of the electrode and the electrolyte solution resulting in an electrical signal. As the HMIs have specified redox potentials, selective determination of certain HMIs can be obtained without using a molecular identification probe utilizing bare electrodes. The anodic stripping voltammetry (ASV) approach, in particular, is being investigated for heavy metal identification. In this, the heavy metals are deposited on the electrode surface followed by stripping or dissolving of the analytes, which are deposited on the electrode surface, which are the two phases in ASV analysis. For example, Wei et al. fabricated a sensor based on SnO₂/graphene oxide nanocomposite for the detection of Hg(II), Cd(II), Cu(II), and Pb(II) in drinking water [128]. Neog et al. developed a WS₂ nanosheets-based sensor to detect Zn(II) [129]. Hui et al. developed a titanium carbide (Ti₃C₂Tx) and multiwalled-carbon-nanotubes (MWNs) nanocomposites based sensor to detect Zn(II) and Cu(II) ions [30]. Pifferi et al. fabricated a sensor based on rGO sheets, functionalized surface with 1-pyrene carboxylic acid, and loaded in situ by gold nanoparticles to determine As(III) ion [130]. A traditional electrochemical sensor has a single response signal, and this has limited the reproducibility due to a variety of parameters such as different properties of the base electrode (i.e., area, morphology), the density of probe loading, and complex detection environments. Due to the virtues of high interference and better reproducibility, the ratiometric technique, a detection mode commonly used in fluorescence research, has been utilized in electrochemical sensors to overcome these challenges [131]. In contrast to traditional single-signal electrochemical sensors, ratiometric electrochemical sensors (RESs) possess two electrochemical signals and utilize the ratio between the two signals as the output signal rather than the single signal absolute value. Therefore, RESs require precise dual electrochemical signal selection, which is a significant design aspect [132]. Many RESs based on 2D materials have been developed to determine various analytes. For example, Xu et al. constructed a ratiometric-antifouling electrochemical biosensor based on multifunctional peptides and MXene with gold nanoparticles and methylene blue for detecting prostate-specific antigen and thrombin [133]. Qu et al. developed a

ratiometric electrochemical platform for detecting ascorbic acid with excellent selectivity, high sensitivity, and good reproducibility by tailoring oxygen-containing groups on graphene [134]. Wang et al. developed a ratiometric electrochemical immuno-sensor for sensitive determination of Human epidermal growth factor receptor-2 using reduced graphene oxide and polydopamine grafted ferrocene/Au@Ag nanoshuttles performing as an electrode material and a hollow Ni@PtNi yolk-shell nanocages-thionine as the signal tags, which measured distinct electrochemical signals for Fc and Thi, respectively [135]. Zhong et al. used MXene on Ag nanoclusters and amino-functionalized multi-walled carbon nanotubes composite to create a new ratiometric electrochemical sensor for the detection of carbendazim [136]. Urgunde et al. performed simultaneous detection of dopamine and uric acid using NiCo₂O₄ on a printed biosensor chip with low LOD and high sensitivity [33].

Different types of 2D materials are widely used for varying electrochemical applications. Among various layered 2D materials, Graphene is highly explored for many electrochemical applications due to its unique properties. It is a one atom thick layer comprising six sp² carbon atoms connected in a honeycomb fashion. Usually, it is used in the pristine form as a support system due to its high surface area and conductivity. It is also used in Graphene Oxide (GO) and reduced form as reduced Graphene Oxide (rGO). GO has the advantage of forming suitable dispersions in polar solvents due to polar oxygen functional groups. But this also leads to decreased electrical conductivity. Direct application of graphene suffers from issues like agglomeration and low sensitivity. Therefore, nanomaterials-based graphene systems are used to overcome these problems. Various graphene and its derivatives-based electrochemical sensors have been reported throughout the literature. For example, Santos et al. developed a laser-induced graphene-based sensor for the selective and sensitive detection of dopamine [137]. Recently Xian et al. reported a Zr-based MOF and graphene composite to determine Ciprofloxacin (CIP) in water by depositing Cu²⁺ ions on the electrode. In the presence of Cip, a complex is formed with Cu²⁺, which results in the decrease of the oxidation current of Cu ions. A limit of detection of 6.67 nM was reported with an excellent linear range of 0.02–1 μM [138]. Graphene oxide nanocomposites can also be utilized in the selective detection of HMIs because of the affinity of metal ions to form bonds with -COOH groups present on the Graphene oxide surface. Rahman et al. used a functionalized graphene oxide and Ag nanowire to detect Hg²⁺. The sensor demonstrated excellent selectivity towards Hg²⁺ ions even in the presence of Cd²⁺, Pb²⁺, Na⁺, Cu²⁺, and Ag⁺. Hg²⁺ has a higher reduction potential,

resulting in easy bond formation with $-\text{COOH}$ groups. Therefore the electrode was highly selective towards Hg^{2+} ions with a detection limit of ~ 0.1 nM with a linear response of 1–70 nM and high sensitivity of 0.29 $\mu\text{A}/\text{nM}$ [63]. Scandurra et al. also fabricated a low-cost disposable sensor of Graphene Paper-Nafion-Bi Nanostructures for Ultra-Trace detection of Pb^{2+} and Cd^{2+} . The sulfonic groups in Nafion get reduced partially to $-\text{SH}$ and organic-sulfides during electrodeposition of Bi. These negatively charged sulfonic groups with reduced thiol groups help bind Pb^{2+} and Cd^{2+} ions, improving the limit of detection. A LOD of 0.1 ppb with a 5–100 ppb linear range was reported [139]. Pizzaro et al. fabricated a green and inexpensive electrochemical sensor using graphene quantum dots and Nafion to determine Cd^{2+} and Pb^{2+} . The selective permeability of positive ions of

Nafion, with the high number of active sites due to graphene QDs, also results in an excellent electrochemical response with LOD of $8.49 \mu\text{g L}^{-1}$ for Pb^{2+} and $11.30 \mu\text{g L}^{-1}$ for Cd^{2+} with a linear range of 20–200 $\mu\text{g L}^{-1}$ [140]. Deshmukh et al. reported a Red Mud-Reduced Graphene Oxide-based electrochemical sensor for Arsenic detection. An excellent limit of detection of 0.07 ppb with a linear range of 0.1–2.3 ppb was found. These results can be attributed to the superb absorption proficiency of hematite-rich Red mud [141]. In Fig. 7a–c Bahuguna et al. performed single-step electrophilic fluorination of SnO_2 for photoelectrochemical application [142]. Borophene is a non-planar buckled molecule with hexagonal vacancies. Limited literature is available due to its toxic starting material, diborane. It is considered superior to graphene in flexibility, strength, and conductivity. Borophene is postulated as a promising material for gas



sensing applications. A lot of computational studies have been done in this area. Recently Shukla et al. presented a computational study for sensing various gases, including CO, NO, NO₂, NH₃, and CO₂. They reported good binding energies for all gases except CO₂ [143]. More computational literature can be found for other molecules like formaldehyde [144] and hydrogen cyanide [145]. Some recent publications have also reported a few non-enzyme borophene-based biosensors. Güngör et al. have reported a Copper phthalocyanine-borophene nanocomposite for urea sensing with a detection limit of 0.05 μM in a linear range of (250–1000) μM [146]. Taşaltın reported a sensor for glucose based on PAN: borophene composite with a detection limit of 0.099 mM [147]. Borophene has a lot of potential in gas sensing applications looking at current computational studies. But due to its susceptibility to oxidation at ambient conditions and toxic starting materials, research is still limited.

Among 2D materials, metal, non-metal and metal-free nitrides are also used in electrochemical sensing due to their good chemical stability, availability, electronic structure, and adjustable bandgap. Among non-metal nitrides, Graphitic carbon nitride (GCN) is quite studied, and many researchers have applied it for heavy metal ion detection [148]. Wang et al. reported porous form S-doped C₃N₄ tubes/ graphene nanosheets to detect Cd²⁺, Hg²⁺, and Pb²⁺ electrochemically. Good LOD was observed due to synergy between hierarchical porous tubes and sulfur doping. The LOD was 1.17, 0.61, and 0.38 nM for simultaneous detection of Cd²⁺, Hg²⁺ and Pb²⁺. Chen et al. used AuNPs/mpg-C₃N₄ nanocomposite to detect methylmercury. Here GCN provides a large surface area for adhesion of gold nanoparticles providing good LOD values [149]. Kokulnathan et al. used Titanium Carbide/Boron Nitride Nanocomposite for sulfadiazine sensing. Low charge transfer resistance (20 ohms), good peak potential separation (0.080 V), and good surface area (0.106 cm²) were observed. LOD of 3 nM was reported [150]. Chen et al. used defect engineering to detect H₂O₂ using self-assembled PGP (polycrystalline GaN porous layers). Self-assembly at low temperature resulted in N-vacancies which improves electrical conductivity. LOD of 50 nM was reported with a fast response speed of 3 s [151]. Liu et al. grew n-type GaN micropillar on p-type GaN substrate electrodes to detect Ag⁺ and Cu²⁺ ions simultaneously. LOD of 3.3 ppb for both ions was reported [152]. MXene is another 2D material with unique properties in sensing applications. In Fig. 5d, f, Park et al. used Ti₃C₂T_x with MWCNTs for Cu and Zn detection. The improved performance was attributed to the increased surface incorporating the MWNTs as anti-pile layers, which removed the

aggregation problem between Ti₃C₂T_x layers and led to a more exposed surface area. In situ Sb deposition was also performed to improve the detection limit further. Low detection limits of 1.5 ppb and 0.1 ppb were reported for Zn and Cu, respectively [30]. Xu et al. used functionalized peptides with Mxene decorated with methylene blue and Au nanoparticles to develop ratiometric antifouling electrochemical biosensors. Accurate prostate-specific antigen detection was reported with a limit of detection of 0.83 pg/ml and a detection range of 5 pg/ml to 10 ng/ml [79]. Yi et al. used Ti₃C₂T_x nanoribbons for HMIs detection using Cd²⁺ as a representative element. A self-reduction strategy was used in place of electrodeposition in the ASV sensing. A low LOD of 0.94 nM with a wide linear range of 0.005–3.0 μM was reported [153]. Xu et al. reported HRP/Ti₃C₂/Nafion film detecting H₂O₂ in patients' serum samples with acute myocardial infarction. A catalytic effect of HRP on H₂O₂ was observed. LOD of 1 μM and a linear range of 5–8000 μM [154]. Gul et al. developed a 2D Nb₂C MXene-based sensor for hydrazine electrochemical sensing [155]. Rasheed et al. reported a sensor based on Pd@Ti₃C₂T_x nanocomposite to detect L-cysteine. The MXene acted as a conductive matrix and a reducing agent at the surface of the electrode, and PDNPs improved the stability of Ti₃C₂T_x. The detection limit of 0.14 μM with a linear range of 0.5–10 μM [156].

Transition metal dichalcogenides represent another class of layered materials used in electrochemical sensing. MoS₂ has been widely studied in this area due to its structural properties. Hwang et al. reported electrochemical detection of Pb²⁺ using MoS₂ nanofilms. Vertical alignment of MoS₂ films performed better as compared to horizontally aligned MoS₂. This sensor showed excellent sensitivity towards Pb²⁺ concentration with an improved LOD of 0.3 ppb with a linear range of 0–20 ppb [157]. Lee et al. reported a sensor based on MoS₂ and graphene composite to detect morin electrochemically. Graphene provides a support system to increase active surface area to increase electrochemical performance [158]. Yuan et al. reported a NiS₂ microblock, MoS₂ nanosheets, and rGO for electrochemical detection of Bisphenol-A. The synergy effects of NiS₂/MoS₂/rGO provided increased conductivity and sensitivity. A lower detection limit of 2.1 nM with a linear range of 0.02–200 μM was reported [159]. Zhou et al. used defect and phase-engineered Mn/MoS₂ nanosheets for heavy metal ion detection. Mn- mediation resulted in a new defect-rich 1 T-MoS₂ form 2H-MoS₂, with better electrical conductivity [160]. References using VS₂ and WS₂ have also been reported in the literature. Yuan et al. developed 2D VS₂/VC/N-Doped carbon sheets loaded with ultrafine-Pd nanoparticles for H₂O₂ sensing. These particles were

assembled on carbon-fiber microelectrodes in a 3D array. This setup improved the electron transfer ability, stability, electrocatalytic activity, and biocompatibility with a LOD of 50 nM [161].

4.4 Electrocatalysis

Currently, research for the development of electrocatalysis using 2D layered materials has been increasing. Some of the emerging 2D layered materials for electrocatalysis include metal oxides (MO_x), nitrides of carbon and boron (CN/BN), 2D metal-organic frameworks (MOFs), transition-metal chalcogenides/dichalcogenides (TMCs/TMDs), 2D covalent organic frameworks (COFs), black phosphorus, MXenes, and layered double hydroxides (LDHs). Compared to their bulk equivalents, the 2D materials show some exceptional properties. These nanosheets possess extraordinary physiochemical properties such as high specific surface area, tunable active sites, etc., enabling them to serve as promising electrocatalysts for different electrochemical processes.

Electrochemical Water Splitting (HER and OER) In Fig. 7d, f, Kang Lim et al. demonstrated that $\text{Mo}_2\text{CT}_x/2\text{H-MoS}_2$ nanohybrids are prepared by an in-situ process via a two-step mechanism sulfidation occurs and the extrinsic oxide layers on Mo_2CT_x are converted to 2H-MoS_2 . This strongly-coupled nanohybrid electrocatalyst shows enhanced HER performance at -10 mA cm^{-2} current density in $0.5 \text{ M H}_2\text{SO}_4$, requiring only 119 mV overpotential [162]. Zepeng et al. fabricated $\text{Co}_2\text{P/N@Ti}_3\text{C}_2\text{T}_x\text{@NF}$ in which cobalt phosphates were grown on MXene ($\text{Ti}_3\text{C}_2\text{T}_x$)-modified Ni foam (NF) in a controlled manner by a two-step electrodeposition process. It exhibited an ultralow overpotential of 15 mV at a current density of 10 mA cm^{-2} [164]. Xu et al. prepared a hierarchical shell on the superficial layer of the metal-organic frameworks (MOFs) using interconnected and vertical Ni-Fe-Ce-LDH nanosheets. It showed an excellent OER performance at a current density of 10 mA cm^{-2} , exhibiting a low overpotential of 242 mV, and at least 24 h durability was shown [165].

Electrochemical Nitrogen Reduction (ENR) Ammonia is greatly significant to industries and humankind in general. Global NH_3 production got as far as 146 million tons in 2015, and by the year 2050, it is likely to increase by 40% [166]. Over 80% of NH_3 total production is used for fertilizers which help sustain lives worldwide [167]. For most industrial chemicals, NH_3 is used as primary raw material, for example, in pharmaceuticals, plastics, dyes, explosives, resins, and synthetic fibers. Also, it has a high energy density and high hydrogen content of 5.52 kWh kg^{-1} and 17.6 wt%, respectively, making it an excellent carbon-free energy carrier [111]. It can be liquified with

ease for transportation and storage and is considered an alternative fuel for H_2 storage.

However, the current ammonia synthesis still depends on the energy-intensive Haber-Bosch process, which needs a high temperature of $\sim 300\text{--}500 \text{ }^\circ\text{C}$ and a high pressure of 150–200 atm. With massive amounts of natural gas consumption and emission of CO_2 . Therefore, developing an approach that is green and sustainable for NH_3 synthesis is quite critical. For their growth, many plants convert atmospheric N_2 into NH_3 fertilizer by an enzyme called nitrogenase. However, due to the ultralow reaction rate of nitrogenase in the artificial N_2 fixation process, research is aimed toward the development of other approaches which can be more advantageous. Catalytic synthesis of NH_3 can be conducted under ambient conditions. Hence, photocatalytic and electrocatalytic N_2 reduction reactions are more effective methods [168].

Electrochemical Nitrogen Reduction (ENR) appears to be a promising research area over the last few years [111]. It is an energy-efficient alternative as it can be driven by electricity from renewable energy sources like solar and wind energy. Nevertheless, ENR suffers from some significant challenges, such as the inert nature of $\text{N}\equiv\text{N}$, the low solubility of N_2 in water, and competing hydrogen evolution reactions. Designing effective electrocatalysts that show a desirable electrocatalytic performance reduces the high activation barrier of the $\text{N}\equiv\text{N}$ bond and shows selectivity towards NRR, decreasing the competing HER is challenging. Various catalysts based on 2D transition metals and their oxides, nitrides, and carbides have been proposed for electrochemical NRR. But the exhibition of low overpotential, high Faradaic efficiency, and long stability and durability is still beyond reach. Zhang et al. reported electrocatalyst Fe doped SnO_2 (Fe-SnO_2) for ambient NRR, which exhibited a remarkable yield of $82.7 \text{ mg h}^{-1} \text{ mg}_{\text{cat}}^{-1}$ and faradaic efficiency (FE) of 20.4% for NRR using the acid electrolyte. Apart from this, it served as an excellent electrocatalyst for NOR, showing a NO_3^- yield of $42.9 \text{ mg h}^{-1} \text{ mg}_{\text{cat}}^{-1}$ and 0.84% FE [169]. Guo reported that MXene/ TiFeO_x -700 nanosheets with modified surfaces showed an excellent FE of 25.44% and $21.9 \text{ } \mu\text{g mg}_{\text{cat}}^{-1} \text{ h}^{-1}$ NH_3 yield. This enhanced performance was due to its high surface reactivity obtained by removing inactive F^*/OH^* terminals and adding Fe to reduce the work function [170]. Peng showed that carbon nitride with N-defects coated on C paper, synthesized at $600 \text{ }^\circ\text{C}$ (CN/C600), demonstrates promising nitrogen reduction activity. It achieved an NH_3 yield of $1.7 \text{ } \mu\text{g mg}_{\text{cat}}^{-1} \text{ h}^{-1}$ with a high FE of 62.1% at -0.1 V vs RHE because of abundant vacancies [171].

CO_2 reduction reaction (CO_2RR): Mesoporous SnO_2 nanosheets (mp-SnO_2) reported by Han et al. when evaluated as CO_2RR electrocatalyst in 0.5 M NaHCO_3

exhibited a high FE of 83% at -0.90 V and great stability for production of formate [172]. Yuan et al. reported that 2D amorphous SnO_x from liquid Sn-Bi alloy containing fine nanoparticles and single atoms of Bi shows high formic acid FE ($>90\%$) in CO_2RR . It also displayed a stable performance over 10 h [173]. Jing Li et al. showed that SnO_2 nanosheet in a traditional H-type electrochemical cell exhibited a FE $>80\%$ over a large potential window for formate production in CO_2RR . A three-compartment microfluidic flow cell electrolyzer can achieve 94.2% high FE and 471 mA cm^{-2} current density (Fig. 8) [174].

4.5 Nanofluidics

Nanofluidics easily find applications in electrochemical energy conversion and storage, biosensing, and water purification. The field of 2D nanofluidics is receiving growing interest due to its high versatility, high scalability, and precise and tunable channel size with different types of 2D nanomaterials. The 2D membranes can be used smartly to control the fluid flow through the nanofluidic channels by switching them completely on and off with high efficiency. Fluids such as electrolytes show drastically different flow properties when confined in nanochannels. Two dimensional (2D) nanosheets dispersed in solution on filtration result in a lamellar structured membrane after restacking and drying. The stacked sheets spontaneously form inter-connected nanochannels of sub-nanometer to a few nanometers size which is also comparable to the size of hydrated ions. The 2D layered membrane needs to have high, stable, and modulable

ionic conductivity [175]. The ion transport through the membrane is largely dependent on the surface properties of the nanochannels, providing a broad range of properties [176]. In 2D nanochannels when the gap/spacing is shorter than the Debye length of the electrolyte, the surface charges on the walls repel ions of the same charge and attract the oppositely charged ions, making them the dominating charge carriers in contrast to bulk solution, where ions move in opposite directions generating ionic current. Such ionic transport phenomena can increase ionic conductivity up to several magnitudes. A two-order enhancement in ionic conductivity (1 Scm^{-1}) of alkali metal ions in two-dimensional MoS_2 nanosheets is observed in contrast with traditional strong ionic materials [187]. Further, MoS_2 membrane-based nanofluidic device in which ionic current is enhanced with light intensity is shown in Fig. 7h, i [109]. It is demonstrated in the literature that the electrical properties of 2D materials, the mass transport can be switched between ultrafast to complete blocking [177], and the ion diffusion can be modulated with low voltage [178]. The functionalized MoS_2 in ultralow concentration can act as a nanofluid decreasing the interfacial tension, changing the contact angle from 131.2° to 51.7° , and imparting emulsion stability by adsorbing at oil/water interfaces [179]. Further, the direction of ion transport and ionic current rectification effect can be reversed with hybrid 2D materials with different surface charges. This includes reconstructing 2D layered materials by asymmetric structure by changing the order in which layers are deposited over one another. For example, the preferential direction for ion transport is reversed by altering the WSe_2 and MoS_2 layers. The ionic current rectification effect in 2D nanofluidic heterostructures provides further opportunities for innovative nanofluidic devices and materials [180]. Free-standing Boron Nitride membranes can be used to fabricate parallel slit-shaped ionic nanochannels with a highly negative zeta potential of $-33.9 \pm 0.9 \text{ mV}$ ($\text{pH} \sim 7$) [181]. LDH (Layered Hydroxide) coating membrane with a conductive polymer allows high ionic conductivity and enhanced selectivity through nanochannels [182]. Polydopamine with excellent ion affinity is coated on the surface of 2D layers to form composite conductive materials with enhanced electric and ionic conductivity [183]. There are many problems associated with the control of fluid flow through nanochannels such as complex preparation of membrane and the lack of charge density stability in the aqueous medium. The composite membrane of cellulose nanofiber with MXene nanosheets shows high tensile strength (171.2 MPa) and aqueous stability and is used for the fabrication of elevated osmotic conversion devices [184]. In literature, various efforts have been made to control the orientation of nanochannels. For example,

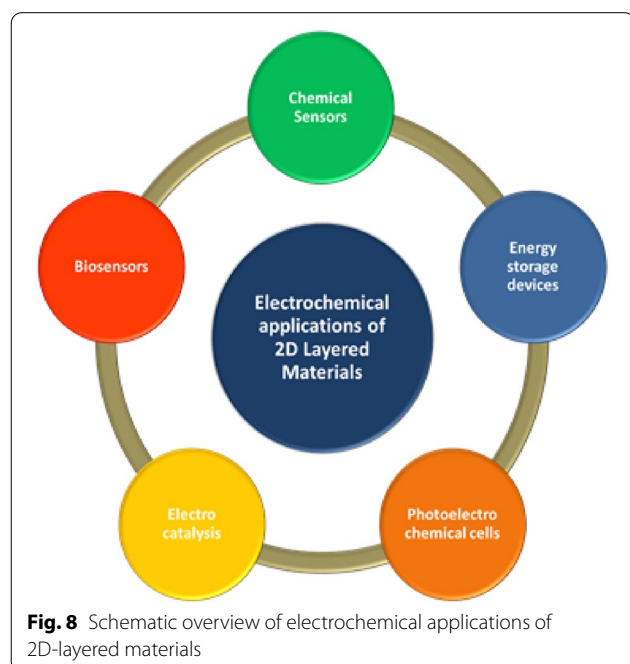


Fig. 8 Schematic overview of electrochemical applications of 2D-layered materials

Zirconium—Graphene Oxide composite is designed with Z-directional transport of ions for improving the thermal stability and molecular selectivity of graphene oxide [185]. Conventional nanofluidic sieving devices fabricated with three-dimensional nanostructures restrict the molecules to ~ 20 nm, while two-dimensional materials offer a sieving resolution of ~ 0.6 nm, which is remarkable. A nanofluidic sieving device is fabricated using hexagonal boron nitride and in-plane graphene recently with an ultrahigh-resolution to separate a single nucleotide [186]. A further implication of nanofluidics in particle transport applications requires 2D materials with enhanced ionic conductivity, stability in different environmental conditions along with patternable and adaptability for miniaturization.

4.6 2D material as memory devices

An increase in the demand for storage capacity and miniaturization of the devices has fueled the research on low dimensional materials for the realization of the von Neumann architecture having independent logic and memory devices. In the recent past, Complementary Metal Oxide Semiconductor is also known as CMOS technology (and is the most accepted technology for design, integration, and manufacturing of the integrated circuits) based on the conventional silicon field-effect transistor (FET) [188] fails to deliver at nanometer technology. In addition, conventional memory devices such as SRAM (Static Random-Access Memory), DRAM (Dynamic RAM), and flash memory are also facing crucial challenges such as power dissipation, robustness, reliability, time-based performance degradation, low on/off ratio, etc. [189–192]. Therefore, Ferroelectric Field Effect Transistors (Fe-FETs), Magnetic Random Access Memory (MRAM), Resistive RAM (RRAM), Phase-Change RAM (PCRAM), and Mem-resistor have been significantly engineered and developed as plausible non-volatile memory device technologies. Interestingly, IBM and 3D-Xpoint have developed and designed memory devices based on spintronics, which is currently being envisaged as an alternative to MRAM [193–195]. However, the challenges such as cost, efficiency, shelf-life, speed, and on/off ratio still need significant improvisation to realize these memory-based upcoming devices. 2D materials having achievable electrostatic gate control such as graphene, transition metal dichalcogenides, phosphorene, and other heterostructures as a semiconducting channel have shown promising results in outcome Si-based FETs [196–209] and with unique intrinsic properties (magnetic moment/electric dipoles) for flash memory devices.

2D material-based flash memory was first reported by Zhan et al. [188] by using graphene (a monoatomic thick sheet of the carbon atom, arranged in a hexagonal

pattern) on a silicon/silicon oxide (Si/SiO_2) layer on a substrate having hafnium oxide on top of the graphene sheet and nickel nanoparticles embedded in the between two layers of hafnium oxide. It was observed that the on/off ratio of the device was poor and the consumption of energy is significantly high as compared to other flash memory devices. This experiment attests to the capacity of the 2D materials as flash memory and opened a new domain of research in the field of layered materials. Later in 2013, Yang et al. investigated the flash memories in memristors and reported that they have a memory retention time of 10 years and have an ultra-fast writing speed of ~ 10 ns. [189] Moreover, with the invention of transition metal dichalcogenide having a bandgap of the order of ~ 1.4 to ~ 1.9 eV (depending upon thickness), a graphene and molybdenum disulfide floating gate flash memory device was realized by Gurarsalan et al. [190]. It was observed that the on/off ratio and energy consumption was dramatically reduced in comparison to the report by Zhan et al. Moreover, many researchers such as Zhang et al. [191], Li et al. [192], and Feng et al. [193] have worked on a similar kind of floating gate TMDCs device using the structure as $\text{MoS}_2/\text{Al}_2\text{O}_3/\text{HfO}_2/\text{Al}_2\text{O}_3$, $\text{BP}/\text{h-BN}/\text{MoS}_2$, and $\text{BP}/\text{Al}_2\text{O}_3/\text{HfO}_2/\text{Al}_2\text{O}_3$ respectively. Although flash memories are well established for layered 2D materials, power consumption for the frequent refresh was the most challenging problem being faced and needs to be overcome. Semi-floating gate memory devices were seen as one of the alternatives to flash memory-based devices and soon made their inception in 2018 by Liu et al. [194]. It was the first report on the quasi-non-volatile memory devices and opened a new paradigm of applications using 2D materials. Liu et al. demonstrated the device performance by using tungsten selenide (WSe_2) /molybdenum disulfide (MoS_2) / boron nitride (h-BN)/hafnium oxide (HfO_2) structure. The heterostructure structure was designed such that the charges from the WSe_2 - MoS_2 layer formed a 2D p–n junction thus transportation of charges can be made swiftly. In addition, the role of the HfO_2 layer was to limit the transfer of charge from the floating gate thus decreasing the power consumption and increasing the operation speed. Although the writing speed was enhanced in the single floating gate devices, the erase speed was now a challenge to overcome. Li et al. in 2019, [195] overcame this challenge by introducing 2D material p–n junction floating gate of WSe_2 - MoS_2 .

Before discussing the FETs that have circuit complexity and usually have high power consumption due to the presence of the oxide layer in comparison to two terminal floating devices. It would be advised to know about the two-terminal memory devices. In FET, the presence of the oxide layer further restricts the growth

in the Z direction (vertically) and limits the flexible nature of the devices [196–210]. However, the two-terminal devices have extremely short channel lengths and the absence of a gate electrode makes them a promising memory device. The two-terminal devices are further classified into two types, namely, Phase-change random-access memory (PRAM) and resistive random-access memory (RRAM) [211–213]. In comparison to FETs, the two-terminal devices have a low on/off ratio and off-state power consumption.

Vu et al. [214] 2016 reported a tunneling random access memory device and have demonstrated the performance of the TRAM in comparison with FETs. In addition, Lee et al. [215, 216] designed a heterolayer graphene/h-BN/MoS₂ much similar to that presented by Choi et al. [217]. The seminal report by Lee et al. has used drain field-induced tunneling charge carriers to write and erase. Moreover, the two-terminal device has laid the stepping stone for layered material-based TRAM and was eventually realized that the TRAM has better efficiency, performance, and potential for the upcoming flexible electronics [218–220].

2D materials have been realized as a potential floating gate material and a variety of them have been used as a non-volatile memory or as flash memory to improve the figure of merit of the devices. Graphene as flash memory helps in reducing the gate stack and minimizing the capacitive coupling. Following the success of graphene in the non-volatile memory, most of its cousins such as transition metal dichalcogenides (MoS₂), boron nitride, black phosphorus, etc. have been investigated and thus created a limited 2D material based non-volatile memory devices and their performance in respect to graphene and conventional silicon have been compared and summarized in Table 1.

4.7 Field emission in 2D materials

Field Emission is one of the most demanding upcoming technologies in the field of electronics (flat panel displays, electron microscopy, traveling wave tubes, etc.) driven and governed by quantum tunneling. It involves exposure of materials to high external fields and ultra-high vacuum conditions for the emission of electrons.

Table 1 2D material-based non-volatile memory devices and their performance

Active layer (thickness)/year	Current switching ratio	Set voltage [V]	Retention	Endurance in cycles	Ref./Year
Graphite [2008]	1.5×10^7	4–6	2 weeks	> 103	[209]
Graphene (1–2 L) [2008]	102	~6	24 h	> 105	[210]
Graphitic stripes (~ 10 nm) [2009]	107	3–4	–	2.2×10^4	[211]
GO thin film (~ 30 nm) [2009]	20	0.3–1	104 s	> 100	[212]
GO thin film (~ 15 nm) [2010]	103	2.5	105 s	> 100	[213]
GO (~ 30 nm) [2010]	103	1.6	107 s	100	[214]
GO thin film (50–100 nm) [2011]	103	0.7	–	–	[215]
RGO thin film (20 nm) [2011]	105	7.5	103 s	> 100	[216]
Graphene (1 L) [2012]	106	7	104 s	–	[217]
rGO-ferrocene film (~ 50 nm) [2012]	103	2	103 s	> 103	[218]
RGO-Au [2011]	2	5	103 s	> 20	[219]
MoS ₂ -PVP (70 nm) [2012]	102	3.5	–	–	[220]
PtAg-MoS ₂ nanobelts in PVP [2014]	–	5	DRAM	–	[221]
MoS ₂ /GO hybrid film (~ 100 nm) [2013]	102	1.2	–	–	[222]
GO/MoS ₂ /GO (total ~ 20 nm) [2016]	104	4	104	102	[223]
MoS ₂ -PMMA [2017]	102–103	2	105	105	[224]
MoS ₂ -PVA [2016]	102	3	104	103	[225]
MoOx/MoS ₂ (50–600 nm) [2015]	106	0.1–0.2	104	104	[226]
1 T-MoS ₂ film (~ 550 nm) [2016]	103	0.1	–	103	[227]
CVD MoS ₂ (~ 1 L) [2015]	103	8.3	120	–	[228]
CVD h-BN (~ 3 nm) [2016]	102	0.72	3×10^3	550	[229]
CVD h-BN (5–7 L) [2017]	10	0.4	–	> 350	[230]
BP (~ 3 μm) [2015]	3×10^5	1.5–2	105	–	[231]
p-type Si (bulk) [2010]	7.5	–	–	–	[232]
p-type Si (bulk) [2011]	16.8	–	10 years	–	[233]
Graphene (1 L) [2013]	20	2	1200 s	> 100	[234]

The three principles of working parameters that define the field emission process are (a) semi-classical thermionic emission, (b) quantum mechanical tunneling, and (c) photoemission. Out of the mentioned technique, thermionic emission is a thermally driven process that incorporates thermal energy which often leads to the emission of surface electrons and thus relies on the Joule-heating method [234]. However, in general, in the field emission process, an electron forms a semiconductor surface tunnels through the vacuum under influence of a high external electrostatic field and ultra-high vacuum at the standard room temperature and pressure [235, 236]. This process is called quantum mechanical tunneling and is also recognized as cold emission at room temperature (usually occurs due to the vacant states available at the Fermi level and the applied electric field). Moreover, in photo-emission, the electrons overcome the potential barrier height by absorbing the incident energy source. In the case of photo-emission, the electrons energetically overcome the potential barrier by gaining enough energy from the incident photons. Thus, the incident photon must be energy higher than the work function (in the case of solids) and/or binding energy of ejecting electron [237–239].

Graphene and its cousin such as molybdenum/tungsten/tin/vanadium sulfide/selenide/disulfide, and phosphorene, as well as their hybrids often offers high field enhancement from the edges and localized defect sites due to the low dimensionality and quantum confinement and is thus being pursued with great scientific interest. It was found that the turn-on field for graphene, WS_2 , VS_2 , SnS_2 , $MoSe_2$, Black phosphorus, ZnO sheets, MoS_2-SnO_2 , $MoS_2-MWCNT$, WS_2-rGO , SnS_2-rGO , MoS_2-rGO are 3.5, 2.3, 4.6, 5.01, 7.5, 2.3, 4.2, 2.4, 3.4, 2.7, 2.0, 2.65 and 2.6 $V/\mu m$ respectively (see Fig. 9) [240–252].

However, 2D materials are yet to be used as cold cathodes and yet to be investigated based on the parameters or their performance which include but are not limited to lower turn-on electric field (E_{on}), lesser threshold electric field (E_{thers}), higher maximum current density, higher field emission factor and high current stability with fewer fluctuations. In addition, some seminal reports suggest that these 2D materials are further tuned and investigated by different techniques such as doping, inducing defects, creating vacancies, surface charge tuning, the inclusion of gate voltage, tuning the thickness, inducing thermal effect, hybridization and composites.

5 Future generation devices and sensors

The advent of 2D materials has completely transformed the face of material science and engineering. It also paves the way to approach Moore's law which has otherwise been slowed down due to technological limitations and

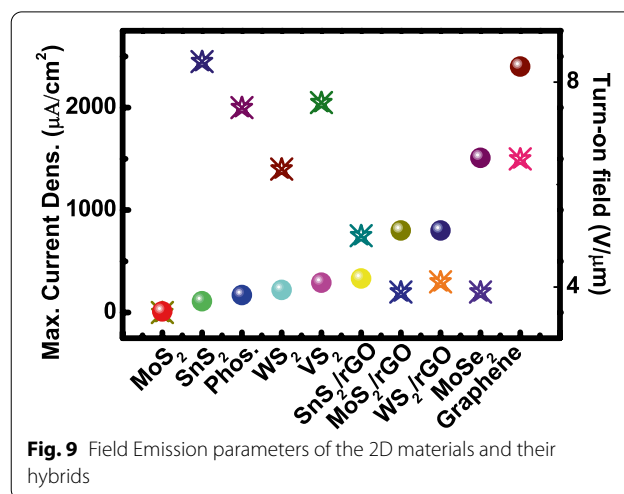


Fig. 9 Field Emission parameters of the 2D materials and their hybrids

fueled the fabrication of next-generation semiconductor devices. In addition, the interesting attributes offered by the members of the 2D materials family and the low power consumption in particular; further augments its frontline applications where nanocrystalline thin films and nanowires miserably failed. It should be noted that the past 30–40 years have seen enormous applications of these nanomaterials of compromised dimensions and off late, it has hit the walls of limitations. 2D materials provide further breathing space and it seems that it has filled the technological gap. Some of the unique characteristics of 2D materials based on the van der Waals and non-van der Waals structure have been explicitly discussed in the article and to summarize the advantage of these advanced materials vis-à-vis their bulk counterpart, numerous scientific data published by leading scientists and researchers, have been collected from the literature and represented in Fig. 10. It is evident from the figure and the discussion in the article that even though graphene in its pure form being a semi-metal has excellent electronic mobility, yet could not exhibit the high ON/OFF ratio, due to lack of carrier concentration and lack of bandgap, other 2D semiconducting cousins do exhibit high ON/OFF ratio. Moreover, doping of graphene and graphene-based hybrids do have the potential for electronic chip applications. Apart from the high carrier mobility (necessary for fast sensing), thermal conductivity (apt to remove extra heat which hampers swift carrier transport), high Young's moduli (good for flexural behavior), and optically transparent nature, these advanced quantum 2D materials have been employed in ultrafast gas/molecular/light/fire/strain sensors, microwave shielding, Flextronics, in hybrid energy storage and mechanically strengthening polymers (see Fig. 10).

2D materials being atomic thick, have unprecedented physical and chemical properties which are better than

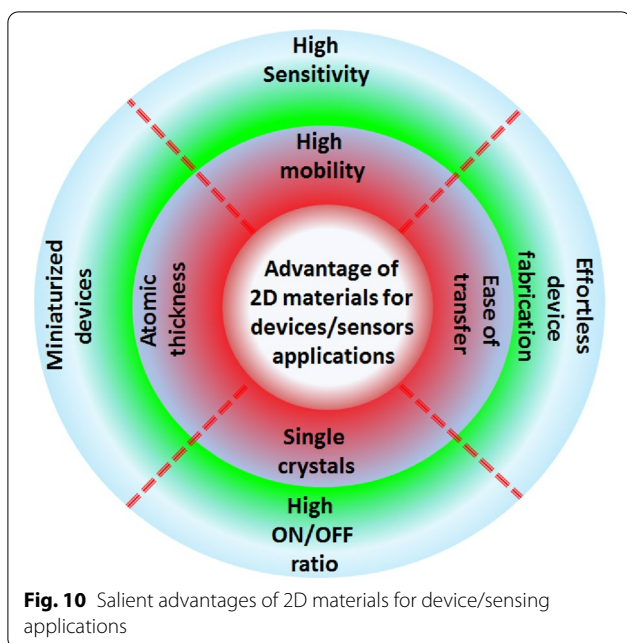


Fig. 10 Salient advantages of 2D materials for device/sensing applications

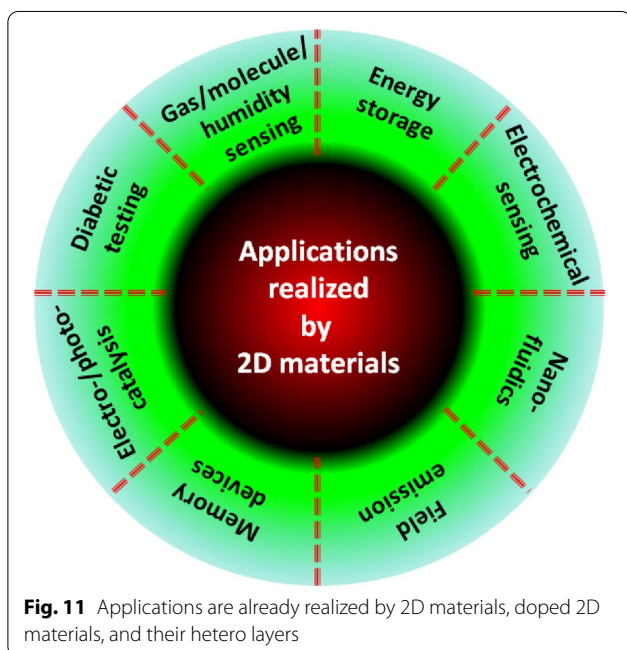


Fig. 11 Applications are already realized by 2D materials, doped 2D materials, and their hetero layers

their bulk counterpart. We have discussed the role of 2D materials from light emission (field emission), and analyte detection to energy generation and storage (Fig. 11). However, the properties shown by the 2D materials can be further enhanced by doping, hybridization, intercalation, and by heterostructure design. In addition, the article also summarizes the synthesis of various 2D materials and their characterization. It should also be mentioned that these 2D materials although seem to be easy to

synthesize, it is difficult to make devices out of them due to certain challenges as discussed in Fig. 14. Amongst various challenges toxicity is one of the issues which need to be addressed. Apart from graphene which originates from carbon, other 2D materials such as alpha lead oxide, phosphorene, and TMDCs are mildly toxic and therefore appropriate precautions in handling are desirable. The other major challenges with these 2D materials during the fabrication of transistors are the lack of current saturation and low current gain. In addition, the pin-hole-free layered devices are free from defects and are suitable to grow on the arbitrary substrate (minimizing mismatch between substrate and film), reusability of the film and substrate, avoiding contact resistance, scalability in synthesis, and larger crystal grain are some of the upcoming challenges which further need to be addressed.

In general, 2D materials has high surface area, high mobility (electron and ionic mobility respectively) high thermal conductivity, structural integrity (especially in borophene and other 2D materials). Some of the 2D materials have atomic scale channels due to ridge line formation in its lattice structure for example borophene, phosphorene, TMDCs etc. which eventually helps in directional electronic or ionic mobility. However, the two critical parameter which generally decide performance and stability of the device (energy storage and generation) are electronic structure and thermal stability. It was found that the specific energy density of the capacitor, supercapacitor and batteries should lie in the range of 0.01–0.1, 0.1–50, 10–200 Wh Kg⁻¹ (as shown in the Fig. 12). In addition, the specific power density, should be 10³ to 10⁷, 1–10⁶ and 10–100 (W Kg⁻¹) respectively, cycling performance be like infinite, >500,000 and 500~2000 respectively and charging time in sec be 10⁻⁶ to 10⁻³, 1–10, 10³ to 10⁵ respectively for capacitor, supercapacitor and batteries (as shown in the Fig. 12).

Numerous applications, challenges and properties of 2D materials need to be investigated before realizing end usage application in terms of devices. A broad perspective to understand and realize these crucial parameter (namely electronic mobility, ionic mobility, young's modulus, thermal conductivity) along with the suitable applications in terms of device performance have been summarized (see Fig. 13). It is evident from the Fig. 13 that the highest electronic mobility can be realized for a device is from graphene. However, it seems that it lags bandgap and thus the ON/OFF ratio is poor which eventually obsolete its use in FETs unless doping or hybridization is being considered with other 2D/3D materials. The ON/OFF ratio of the electronic chip depends on the bandgap of the material and thus other 2D material are being explored with great scientific interest. In light of the ON/OFF ratio it was found that anisotropic materials

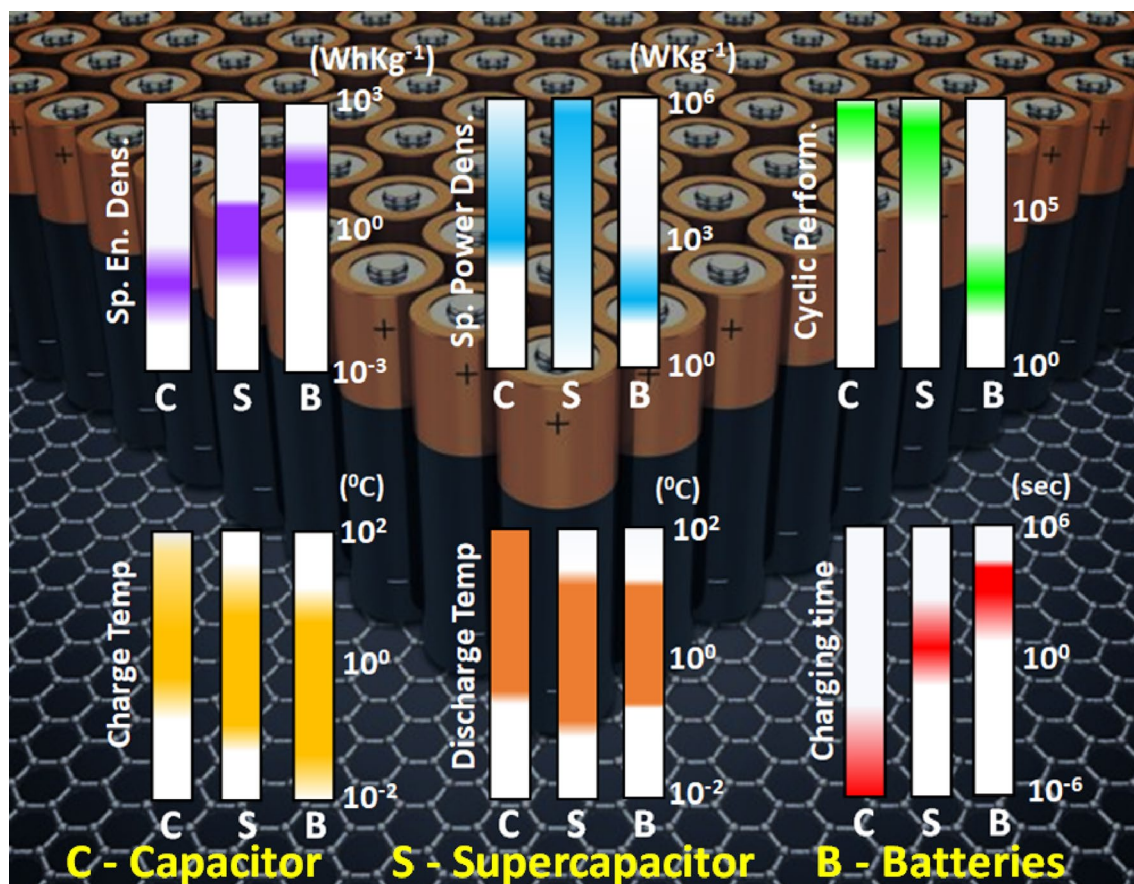


Fig. 12 Summary of critical parameters deciding capacitor, supercapacitor and batteries performance

especially borophene is a promising material for FETs. Xenon ribbons are similarly being investigated for straintronics, gas sensing, and molecule sensing. However, when doped with different atoms its being an interesting material for spintronics, optoelectronics etc. Boron nitride the best insulator being found in the 2D family is currently being a sensation for application in thermal packaging, tunneling barrier and gate dielectric due to high thermal conductivity. TMDCs are apt for band gap engineering based optoelectric applications such as in LEDs and solar cells. MXenes do possess stable structure and band gap adequate for energy storage and water splitting and catalytic CO_2 conversion.

6 Primary challenges

Obtaining defect-free atomically thin crystal is in general difficult. Growing or transferring such crystal on arbitrary substrate is a challenge in itself. Many approaches of synthesis (Bottom-up methods such as MPCVD and laser CVD; Top-down methods such as laser exfoliation, direct exfoliation using PDMS stamp etc.) and adequate lithography (e-beam, ion-beam and laser beam, AFM-tip

based) are therefore being developed to address to these challenges. To have atom-by-atom information, high resolution HAADF HRTEM imaging, atomic-scale elemental profiling via STEM EELS is being employed. XPS and Raman mapping have come very far to diagnose the specific surfaces such as doped Xenon, where local information is desirable. In fact, uniform graphitic doping is desirable, however not very straight forward. Therefore, new ways to attain such uniformity in doping are being developed. Further, new approaches to accomplish strong 2D-2D hybridized materials are being explored. In general, for 2D-2D hybrids, getting interfacial information is difficult. HRTEM, Raman mapping etc. can help diagnose the effect, however exact interpretation is difficult as there are many factors such as Moire potential developed (due to shear, translation, rotation of crystals relative to each other), unwanted stacking, voids/trapped air at the interfaces etc. All these factors give rise to undesirable noises in electrical signal. In fact, room temperature electrical signal is very noisy. Therefore, room-temperature diagnosis tools such as scanning tunneling microscopy (STM) or current force microscopy (CAFM) based

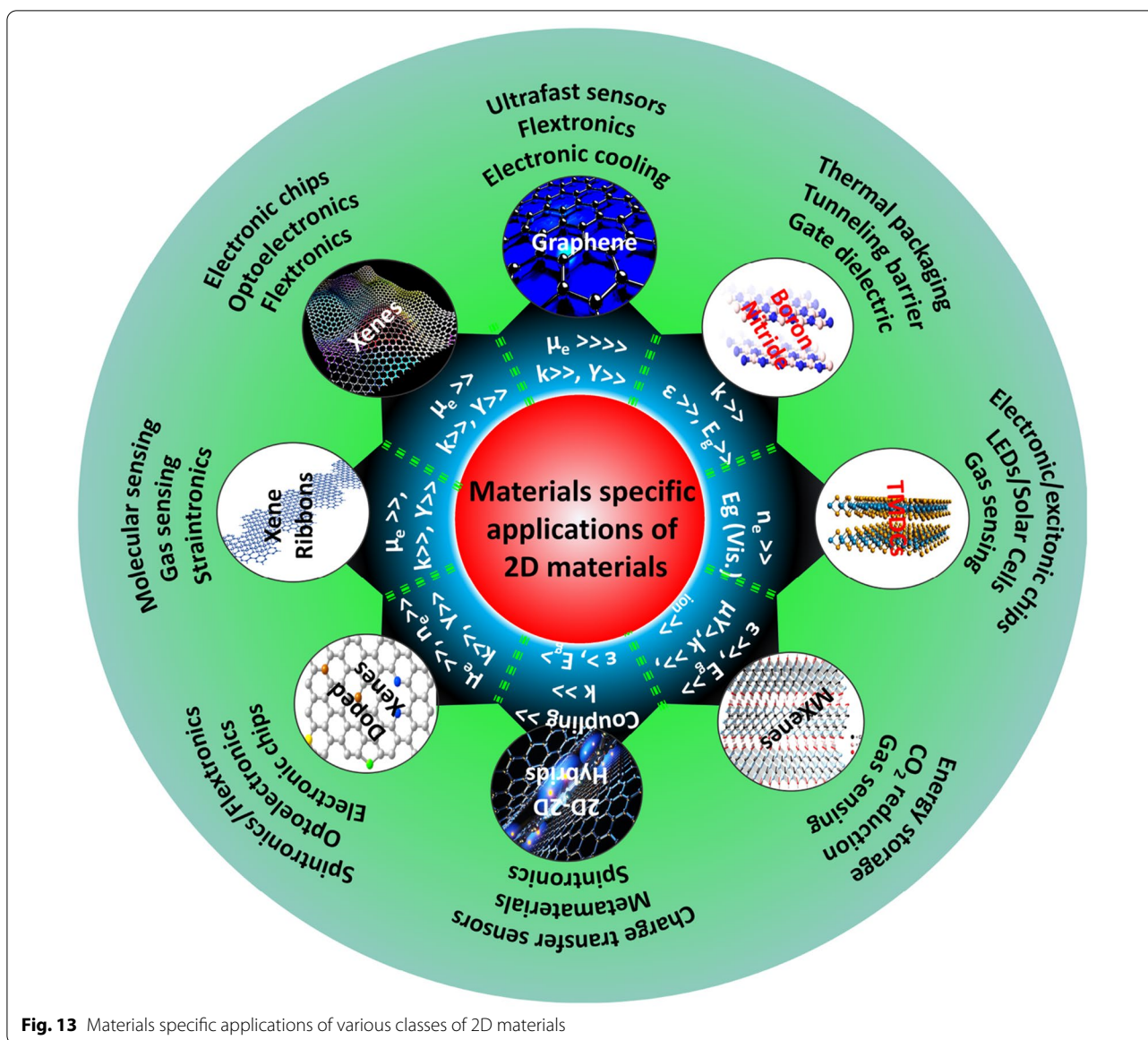


Fig. 13 Materials specific applications of various classes of 2D materials

electrical signals for evaluating the quality of interfaces are being developed [253].

The 2D materials for electrocatalysis need defect engineering to improve catalytic performance and increase the number of active sites and the electronic conductivity of the material. A fundamental understanding of the electrocatalytic behavior of a material and its correlation with defects require further enhancement. The development of multi-functional electrocatalysts is needed by rational defects design and other routes for a clean, sustainable, and low-cost energy conversion [254]. 2D-layered electrode materials in supercapacitors provide excellent areal/volumetric capacitance with high energy density, power density, and long life cycles at a relatively

low cost. The synthesis of a single 2D layer requires multiple-step processes and involves both considerable time and money. The production of high-quality 2D layered material at an industrial scale is a big challenge because of the high chemical activity and storage of 2D materials. The performance of 2D materials is hindered by atmospheric factors like humidity, electrolyte evaporation due to high temperature, and undesirable chemical reactions. The nanocomposites of 2D layered materials with other conducting materials may solve many of these issues with the cost of some drop in performance but are applicable for practical applications in electrocatalysis [255]. In nanofluidics, 2D materials often undergo reduction or cross-linkage instead of forming a desirable laminar

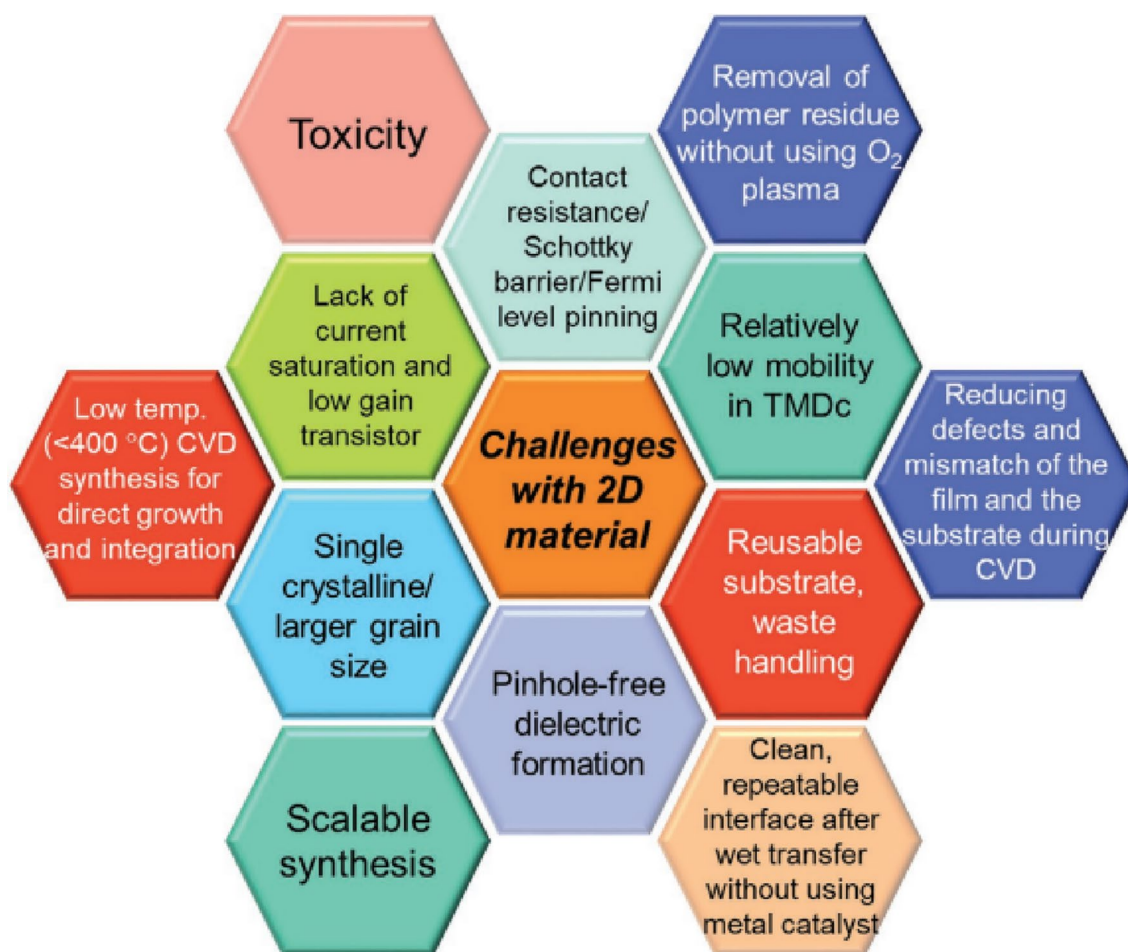
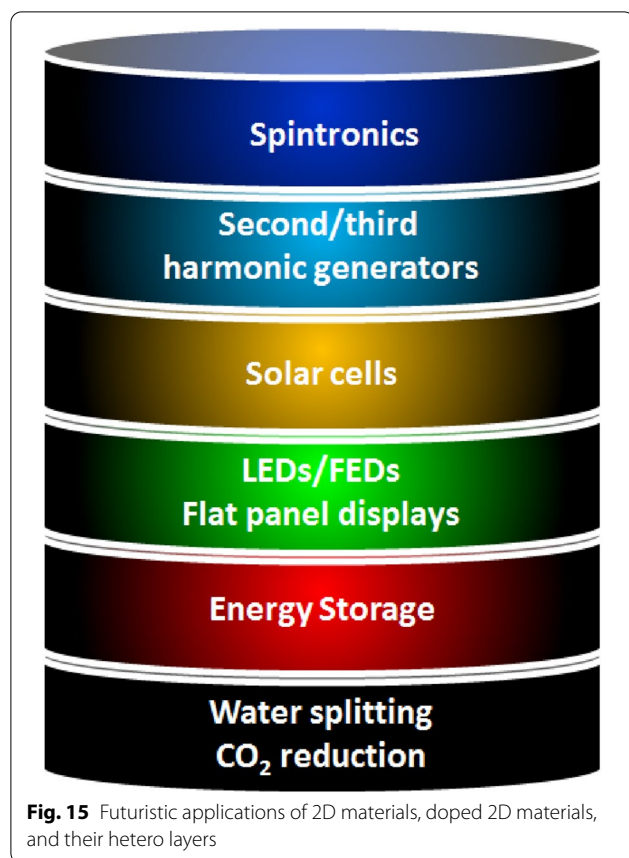


Fig. 14 Challenges faced by 2D materials from synthesis to device applications [50]

structure. In addition, the electrostatic repulsion between nanosheets membrane can disintegrate in the aqueous medium. Moreover, the cross-linkage can change the hydrophilicity, creating undesirable changes in fluid flow [174]. The cost-effective device manufacturing technologies need to be addressed for flexible, miniaturized, and industrial-scale gas sensors [256, 257]. The synthetic strategies which provide reasonable control over the layer thickness, defects, and composition needs to be developed to enhance the selectivity and sensitivity for optimum performance [88]. One of the significant issues with device fabrication is to make ohmic contact between 2D nanomaterials and metal contacts, as it requires sophisticated techniques and skilled labor, which indirectly sums up to increase the device cost [91]. Generic challenges in working with 2D materials are shown in Fig. 14.

Although 2D materials based devices are facing device fabrication challenges due to scalability issues, especially device integration issues, interconnects etc., with new technologies and better understanding of these

material properties they are highly sought after materials for supercapacitors due to high surface area and ionic conductivity, magnetic devices as single doped atoms/functionalities on same lattice and different lattices can induce spin oriented magnetism also called as spintronics, flexible displays due to flexural behavior and also due to optical transparency and tunable electronic bandgap, energy storage due to high specific surface area, water splitting due to control over the kinetics of the material domains, filtration by inducing atomistic level defects which eventually will obsolete analytes such as sodium, potassium etc. and prevent fouling as well as maintains the Young's modulus, lubricants by decreasing the friction due to presence of weak van der Waals force of attraction, second/third harmonic generators, dye adsorbents due to control over surface charge density and distribution etc. (see Fig. 15). Bioelectronics and future lab-on-chip devices based on 2D materials is yet another applications, 2D materials is catching up in recent times [258]. Field emission applications of



2D quantum crystals is extremely interesting from field emission display application point of view [259]. Large scale applications of 2D materials are very promising e.g. in mechanically strengthening glass (for bulletproofs), aluminum (for light combat aircrafts), steel rods (for earthquake resistant residential towers and rust-proof river/ocean bridges), plastic sheets (for various flexural devices/appliances) etc. Thus, we see that within no time, quantum flatland has broadened laterally and has encompassed a myriads of applications.

7 Conclusions

The evolution of the family of 2D materials consisting of monoelemental atomic sheets called Xenos, boron nitride, TMDCs, MXenes, etc. has been described and discussed in detail. Important synthesis protocols for these advanced materials have been summarized. Characterizations of 2D materials have been elaborated with an emphasis on chemical identification and electronic character determination. Salient practical applications of 2D materials primarily in energy storage, gas and humidity sensing, electrochemical sensing, electrocatalysis, nanofluidics, memory devices, and field emission have been discussed. At the end of the review, the future

generation of devices and sensors have been elaborated and a perspective has been presented.

Abbreviations

FESEM: Field emission scanning electron microscopy; AFM: Atomic force microscope; TEM/HRTEM: Transmission electron microscope/ high-resolution transmission electron microscope; XPS: X-ray photoelectron spectroscopy; FTIR: Fourier transform infrared; FET: Field-effect transistor; LEDs: Light emitting diodes; SERS: Surface enhanced Raman spectroscopy; TMDCs: Transition metal dichalcogenides; HER: Hydrogen evolution reaction; OER: Oxygen evolution reaction; MOFs: Metal oxide frameworks; RH: Relative humidity; VOC: Volatile organic compounds; ENR: Electrochemical nitrogen reduction; ppb: Parts-per-billion; ppm: Parts-per-million; RAM: Random access memory; BN: Boron nitride; BP: Black phosphorus; TMOs: Transition metal oxides; MnO₂: Manganese dioxide; NiCo₂O₄: Nickel cobaltite; RuO₂: Ruthenium (IV) oxide; Fe₃O₄: Iron (II, III) oxide; NiO: Nickel oxide; Co: Cobalt; Cu: Copper; MoS₂: Molybdenum disulphide; WS₂: Tungsten disulfide; TiS₂: Titanium disulfide; NbS₂: Niobium disulfide; VS₂: Vanadium sulfide; WS₂-PANI: Tungsten disulfide/polyaniline; kHz: Kilo-hertz; CNT/GO: Carbon nanotube/graphene oxide; CoFe₂O₄: Cobalt ferrite; MWNTs: Multi-walled carbon nanotubes; Au: Gold; PET: Polyethylene terephthalate; NPs: Nano-particles; SnO₂: Tin oxide; WO₃: Tungsten trioxide; MoO₃: Molybdenum trioxide; TiO₂: Titanium oxide; α -Fe₂O₃: Alpha Iron (III) oxide; NH₃: Ammonia; rGO: Reduced graphene oxide; nM: Nanomolar; COOH: Carboxylic acid; SnS₂: Tin selenide; HfO₂: Hafnium oxide; $\mu\text{Wh}/\text{cm}^3$: Micro-watt-hour per centimetre cube; mF cm^{-2} : Milli-farad per centimetre square; A g^{-1} : Ampere per gram; Fg^{-1} : Farad per gram; mVs^{-1} : Milli-volt per second.

Acknowledgements

PR would like to thank the Indian Institute of Technology Jodhpur (IITJ) for the financial support and the SEED grant. SG acknowledges IIT Jodhpur and Prime Minister Research Fellowship, Government of India for fellowship. HY acknowledges MHRD, the Government of India, and IIT Jodhpur for fellowship. AP, KV, and DK acknowledge the Department of Chemistry, IIT Jodhpur. RG and PR thank IDR-IPoT & Application (IITJ) for providing the opportunity to undertake this collaborative work.

Author contributions

Abstract, Introduction and Synthesis were written by PK. Characterizations, electronic/optoelectronic, and memory applications were written by PR. Applications of 2D materials in Energy storage were written by SG, AP, and RG; sensing applications were written by SG, HY, AU, and RG; Catalysis applications were written by HY, VS, KV, and RG; Nanofluidics was written by DK, SG, and RG. Summary and future scope were written by PK and PR. Everyone on the author's list has contributed to review writing. PK, PR, and RG have gone through the whole manuscript. All authors read and approved the final manuscript.

Funding

Science and Engineering Research Board (SERB) with Grant nos. SERB/F/8448/2020-2021 and CRG/2020/003465.

Availability of data and materials

Not applicable.

Declarations

Competing interests

The authors declare that they have no competing interests.

Received: 7 April 2022 Accepted: 22 May 2022

Published online: 06 June 2022

References

1. K.S. Novoselov, A.K. Geim, V. Morozov, J. Zhangs, V. Dubonos, V. Grigorieva, A.A. Firsov, *Science* **306**(5696), 666–669 (2004). <https://doi.org/10.1126/science.1102896>

45. D. Voiry, J. Yang, J. Kupferberg, R. Fullon, C. Lee, H.Y. Jeong, H.S. Shin, M. Chhowalla, High-quality graphene via microwave reduction of solution-exfoliated graphene oxide. *Science* **353**(6306), 1413–1416 (2016). <https://doi.org/10.1126/science.aah3398>
46. P. Kumar, K.S. Subrahmanyam, C.N.R. Rao, Graphene produced by radiation-induced reduction of graphene oxide. *Int. J. Nanosci.* **10**, 559–566 (2011). <https://doi.org/10.1142/S0219581X11008824>
47. K.S. Subrahmanyam, P. Kumar, A. Nag, C.N.R. Rao, Blue light emitting graphene-based materials and their use in generating white light. *Solid State Commun.* **150**(37–38), 1774–1777 (2010). <https://doi.org/10.1016/j.ssc.2010.07.017>
48. P. Kumar, M.G. Krishna, A.K. Bhattacharya, Electric-field-induced nanostructuring of metallic thin films. *Int. J. Nanosci.* **07**, 255–261 (2008). <https://doi.org/10.1142/S0219581X08005407>
49. P. Ranjan, T.K. Sahu, R. Bhushan, S.S.R.K.C. Yamijala, D.J. Late, P. Kumar, A. Vinu, Freestanding borophene and its hybrids. *Adv. Mater.* **31**, 27 (2019). <https://doi.org/10.1002/adma.201900353>
50. P. Ranjan, J.M. Lee, P. Kumar, A. Vinu, Borophene: New Sensation in Flatland. *Adv. Mater.* **32**, 34 (2020). <https://doi.org/10.1002/adma.20200531>
51. S. Chahal, P. Ranjan, M. Motlag, S.S.R.K.C. Yamijala, D.J. Late, E.H.S. Sadki, G.J. Cheng, P. Kumar, Borophene via micromechanical exfoliation. *Adv. Mater.* **33**, 34 (2021). <https://doi.org/10.1002/adma.202102039>
52. T.K. Sahu, P. Ranjan, P. Kumar, Chemical exfoliation synthesis of boron nitride and molybdenum disulfide 2D sheets via modified Hummers' method. *Emergent Mater.* **4**, 645–654 (2021). <https://doi.org/10.1007/s42247-021-00170-0>
53. C. Andrea, Ferrari Raman spectroscopy of graphene and graphite: disorder, electron–phonon coupling, doping and nonadiabatic effects. *Solid State Commun.* **143**, 47–57 (2007). <https://doi.org/10.1016/j.ssc.2007.03.052>
54. P. Ranjan, J. Balakrishnan, A.D. Thakur, Dye adsorption behavior of graphene oxide. *Mater. Today: Proc.* **11**, 833–836 (2019). <https://doi.org/10.1016/j.matpr.2019.03.052>
55. F. Yi, H. Ren, J. Shan, X. Sun, D. Wei, Z. Liu, Wearable energy sources based on 2D materials. *Chem. Soc. Rev.* **47**, 3152 (2018). <https://doi.org/10.1039/c7cs00849j>
56. Y. Da et al., Engineering 2D architectures toward high-performance micro-supercapacitors. *Adv. Mater.* (2018). <https://doi.org/10.1002/adma.201802793>
57. R. Sahoo, A. Pal, T. Pal, 2D materials for renewable energy storage devices: outlook and challenges. *Chem. Commun.* **52**(93), 13528–13542 (2016). <https://doi.org/10.1039/C6CC05357B>
58. C. Meng, P. Das, X. Shi, Q. Fu, K. Müllen, Z.-S. Wu, In situ and operando characterizations of 2D materials in electrochemical energy storage devices. *Small Sci.* **1**(4), 2000076 (2021). <https://doi.org/10.1002/SMSC.202000076>
59. J. Nan et al., Nanoengineering of 2D MXene-based materials for energy storage applications. *Small* (2019). <https://doi.org/10.1002/sml.201902085>
60. Y. Xia et al., Thickness-independent capacitance of vertically aligned liquid-crystalline MXenes. *Nature* (2018). <https://doi.org/10.1038/s41586-018-0109-z>
61. Z. Zhao et al., Scalable 3D self-assembly of MXene films for flexible sandwich and micro-sized supercapacitors. *Adv. Funct. Mater.* (2021). <https://doi.org/10.1002/adfm.202101302>
62. H. Te Ng Ta, W. Sun, L. Wang, and Q. Yan, “Energy-storage materials 2D transition metal oxides/hydroxides for energy-storage applications,” (2015). [Online]. Available: www.chemnanomat.org
63. Z. Ma et al., High-stability MnO_x Nanowires@C@MnO_x nanosheet core-shell heterostructure pseudocapacitance electrode based on reversible phase transition mechanism. *Small* (2019). <https://doi.org/10.1002/sml.201900862>
64. S. Chen, H. Jiang, Q. Cheng, G. Wang, S. Petr, C. Li, Amorphous vanadium oxides with metallic character for asymmetric supercapacitors. *Chem. Eng. J.* **403**, 126380 (2021). <https://doi.org/10.1016/J.CEJ.2020.126380>
65. R.S. Santos, R. Suresh Babu, M. Devendiran, D.B. Haddad, A.L.F. de Barros, Facile synthesis of transition metal (M = Cu, Co) oxide grafted graphitic carbon nitride nanosheets for high performance asymmetric supercapacitors. *Mater. Lett.* **308**, 131156 (2022). <https://doi.org/10.1016/J.MATLET.2021.131156>
66. A. De Adhikari et al., Tungsten-disulfide/polyaniline high frequency supercapacitors. *Adv. Electron. Mater.* **7**(6), 2100025 (2021). <https://doi.org/10.1002/AELM.202100025>
67. S. Venkateshalu et al., Phosphorene, antimonene, silicene and siloxene based novel 2D electrode materials for supercapacitors—a brief review. *J. Energy Storage* **48**, 104027 (2022). <https://doi.org/10.1016/J.EST.2022.104027>
68. Y.K. Kim, K.Y. Shin, Functionalized phosphorene/polypyrrole hybrid nanomaterial by covalent bonding and its supercapacitor application. *J. Ind. Eng. Chem.* **94**, 122–126 (2021). <https://doi.org/10.1016/J.JIEC.2020.10.044>
69. L. Miao, Z. Song, D. Zhu, L. Li, L. Gan, M. Liu, Recent advances in carbon-based supercapacitors. *Mater. Adv.* **1**(5), 945–966 (2020). <https://doi.org/10.1039/d0ma00384k>
70. P. Nakhanivej, Q. Dou, P. Xiong, H.S. Park, Two-dimensional pseudo-capacitive nanomaterials for high-energy- and high-power-oriented applications of supercapacitors. *Accounts Mater. Res.* **2**(2), 86–96 (2021). <https://doi.org/10.1021/accountsmr.0c00070>
71. Y. Zou, I.A. Kinloch, R.A.W. Dryfe, Nitrogen-doped and crumpled graphene sheets with improved supercapacitance. *J. Mater. Chem. A* **2**(45), 19495–19499 (2014). <https://doi.org/10.1039/c4ta04076g>
72. P. Nakhanivej et al., Revealing molecular-level surface redox sites of controllably oxidized black phosphorus nanosheets. *Nat. Mater.* **18**(2), 156–162 (2019). <https://doi.org/10.1038/s41563-018-0230-2>
73. S. Zhu et al., Monolithic flexible supercapacitors drawn with nitrogen-doped carbon nanotube-graphene ink. *Mater. Res. Bull.* **139**, 111266 (2021). <https://doi.org/10.1016/j.materresbull.2021.111266>
74. D.Y. Wu, J.J. Shao, Graphene-based flexible all-solid-state supercapacitors. *Mater. Chem. Front.* **5**(2), 557–583 (2021). <https://doi.org/10.1039/d0qm00291g>
75. G.A.M. Ali, M.R. Thalji, W.C. Soh, H. Algarni, K.F. Chong, One-step electrochemical synthesis of MoS₂/graphene composite for supercapacitor application. *J. Solid State Electrochem.* **24**(1), 25–34 (2020). <https://doi.org/10.1007/s10008-019-04449-5>
76. R. Gupta, A.B. Urgunde, G. Bahuguna, A. Dharmija, P.P. Das, Ni ink-catalyzed conversion of a waste polystyrene–sugar composite to graphitic carbon for electric double-layer supercapacitors. *ACS Appl. Electron. Mater.* **2**(10), 3178–3186 (2020). https://doi.org/10.1021/ACS.AELM.0C00542/SUPPL_FILE/EL0C00542_SI_001.PDF
77. Y. Chao et al., One-pot hydrothermal synthesis of solution-processable MoS₂/PEDOT:PSS composites for high-performance supercapacitors. *ACS Appl. Mater. Interfaces* **13**(6), 7285–7296 (2021). <https://doi.org/10.1021/acami.0c21439>
78. L. Hou et al., In-situ formation of oxygen-vacancy-rich NiCo₂O₄/nitrogen-deficient graphitic carbon nitride hybrids for high-performance supercapacitors. *Electrochim. Acta* **340**, 135996 (2020). <https://doi.org/10.1016/j.electacta.2020.135996>
79. C.K. Maity, S. Sahoo, K. Verma, G.C. Nayak, SnS₂@Conducting energy level-induced functionalized boron nitride for an asymmetric supercapacitor. *Energy Fuels* (2021). <https://doi.org/10.1021/acs.energyfuels.1c04436>
80. J. Rajendran, A.N. Reshetilov, A.K. Sundramoorthy, Preparation of hybrid paper electrode based on hexagonal boron nitride integrated graphene nanocomposite for free-standing flexible supercapacitors. *RSC Adv.* **11**(6), 3445–3451 (2021). <https://doi.org/10.1039/d0ra10735b>
81. C. Sun et al., Self-assembly of alternating stacked 2D/2D Ti₃C₂TxMXene/ZnMnNi LDH van der Waals heterostructures with ultrahigh supercapacitive performance. *ACS Appl. Energy Mater.* **3**(10), 10242–10254 (2020). <https://doi.org/10.1021/acsaem.0c02077>
82. I. Ayman et al., CoFe₂O₄ Nanoparticle-decorated 2D MXene: a novel hybrid material for supercapacitor applications. *Energy Fuels* **34**(6), 7622–7630 (2020). <https://doi.org/10.1021/acs.energyfuels.0c00959>
83. A. Sharma, P. Mane, B. Chakraborty, C.S. Rout, 1T-VS₂/MXene hybrid as a superior electrode material for asymmetric supercapacitors: experimental and theoretical investigations. *ACS Appl. Energy Mater.* **4**(12), 14198–14209 (2021). <https://doi.org/10.1021/acsaem.1c02959>
84. X. Hui et al., High-performance flexible electrochemical heavy metal sensor based on layer-by-layer assembly of Ti3C2Tx / MWNTs nanocomposites for noninvasive detection of copper and zinc ions in human bio fluids. *ACS Appl. Mater. Interfaces* (2020). <https://doi.org/10.1021/acsaem.0c12239>

85. A.B. Urgunde, A.R. Kumar, K.P. Shejale, R.K. Sharma, R. Gupta, Metal wire networks functionalized with nickel alkanethiolate for transparent and enzymeless glucose sensors. *ACS Appl. Nano Mater.* **1**(10), 5571–5580 (2018). https://doi.org/10.1021/ACSANM.8B01115/SUPPL_FILE/AN8B01115_SI_001.PDF
86. A.B. Urgunde, G. Bahuguna, A. Dhamija, V. Kamboj, R. Gupta, Scalable production of nickel cobaltite nanoplates using solution-processed inks for OER electrocatalysis. *Mater. Res. Bull.* **142**, 111380 (2021). <https://doi.org/10.1016/J.MATERRESBULL.2021.111380>
87. A.B. Urgunde, A. Dhamija, R. Gupta, Nickel cobaltite nanoplate-based electrochemical sensing platform from printable inks for simultaneous detection of dopamine and uric acid. *Chem. An Asian J.* **17**(2), e202101166 (2022). <https://doi.org/10.1002/ASIA.202101166>
88. M. Kiani, M.U. Rehman, X. Tian, B. Yakobson, Two-dimensional nanomaterials for the development of efficient gas sensors: recent advances, challenges, and future perspectives. *Adv. Mater. Technol.* (2021). <https://doi.org/10.1002/ADMT.202101252>
89. L. Zhang, K. Khan, J. Zou, H. Zhang, Y. Li, Recent advances in emerging 2D material-based gas sensors: potential in disease diagnosis. *Adv. Mater. Interfaces* (2019). <https://doi.org/10.1002/admi.201901329>
90. Z. Meng, R.M. Stolz, L. Mendecki, K.A. Mirica, Electrically-transduced chemical sensors based on two-dimensional nanomaterials. *Chem. Rev.* **119**, 478–598 (2019). <https://doi.org/10.1021/acs.chemrev.8b00311>
91. A. Bag, N.E. Lee, Gas sensing with heterostructures based on two-dimensional nanostructured materials: a review. *J. Mater. Chem. C* **7**(43), 13367–13383 (2019). <https://doi.org/10.1039/C9TC04132J>
92. T. Yang et al., Atomically thin 2D transition metal oxides: structural reconstruction, interaction with substrates, and potential applications. *Adv. Mater. Interfaces* **6**(1), 1801160 (2019). <https://doi.org/10.1002/ADMI.201801160>
93. D. Wang et al., Mesoporous ultrathin SnO₂ nanosheets in situ modified by graphene oxide for extraordinary formaldehyde detection at low temperatures. *ACS Appl. Mater. Interfaces* **11**(13), 12808–12818 (2019). <https://doi.org/10.1021/acsami.9b01465>
94. C. Qin, B. Wang, N. Wu, C. Han, Y. Wang, General strategy to fabricate porous co-based bimetallic metal oxide nanosheets for high-performance CO sensing. *ACS Appl. Mater. Interfaces* **13**(22), 26318–26329 (2021). <https://doi.org/10.1021/acsami.1c03508>
95. J.-S. Jang et al., Heterogeneous, porous 2D oxide sheets via rapid galvanic replacement: toward superior HCHO sensing application. *Adv. Funct. Mater.* (2019). <https://doi.org/10.1002/adfm.201903012>
96. B. Sun et al., Co₃O₄@PEI/Ti₃C₂T_x MXene nanocomposites for a highly sensitive NO_x gas sensor with a low detection limit. *J. Mater. Chem. A* (2021). <https://doi.org/10.1039/d0ta11392a>
97. H. Zhi, X. Zhang, F. Wang, P. Wan, L. Feng, Flexible Ti₃C₂T_x MXene/PANI/bacterial cellulose aerogel for e-skins and gas sensing. *ACS Appl. Mater. & Interfaces* **13**(38), 45987–45994 (2021). <https://doi.org/10.1021/acsami.1c12991>
98. S. Kim, J. Lee, S. Doo, Y. Chan Kang, C. Min Koo, S. Joon Kim, Metal-ion-intercalated MXene nanosheet films for NH₃ gas detection. *ACS Appl. Nano Mater.* **4**(12), 14249–14257 (2021). <https://doi.org/10.1021/acsanm.1c03814>
99. T. He et al., MXene/SnO₂ heterojunction based chemical gas sensors. *Sens. Actuators B Chem.* **329**, 129275 (2021). <https://doi.org/10.1016/J.SNB.2020.129275>
100. M. Liu, J. Ji, P. Song, M. Liu, Q. Wang, α-Fe₂O₃ nanocubes/Ti₃C₂T_x MXene composites for improvement of acetone sensing performance at room temperature. *Sens. Actuators B Chem.* **349**, 130782 (2021). <https://doi.org/10.1016/J.SNB.2021.130782>
101. G. Bahuguna et al., Innovative approach to photo-chemiresistive sensing technology: surface-fluorinated SnO₂ for VOC detection. *ACS Appl. Mater. Interfaces* **12**(33), 37320–37329 (2020). <https://doi.org/10.1021/acsami.0c08847>
102. B. Kwon et al., Ultrasensitive N-channel graphene gas sensors by nondestructive molecular doping. *ACS Nano* **16**(2), 2176–2187 (2022). <https://doi.org/10.1021/acs.nano.1c08186>
103. D. Li et al., 2D boron sheets: structure, growth, and electronic and thermal transport properties. *Adv. Funct. Mater.* (2019). <https://doi.org/10.1002/adfm.201904349>
104. C. Hou, G. Tai, Y. Liu, X. Liu, Borophene gas sensor. *Nano Res.* **15**(3), 2537–2544 (2021). <https://doi.org/10.1007/S12274-021-3926-6>
105. C. Hou, G. Tai, B. Liu, Z. Wu, Y. Yin, Borophene-graphene heterostructure: preparation and ultrasensitive humidity sensing. *Nano Res.* (2020). <https://doi.org/10.1007/s12274-020-3232-8>
106. J. Shen, Z. Yang, Y. Wang, L.-C. Xu, R. Liu, X. Liu, Organic gas sensing performance of the borophene van der Waals heterostructure. *J. Phys. Chem. C* **125**(1), 427–435 (2021). <https://doi.org/10.1021/acs.jpcc.0c08580>
107. T. Pham, G. Li, E. Bekyarova, M.E. Itkis, A. Mulchandani, MoS₂-based optoelectronic gas sensor with sub-parts-per-billion Limit of NO₂ gas detection. *ACS Nano* **13**(3), 3196–3205 (2019). <https://doi.org/10.1021/acsnano.8b08778>
108. K. Yong Ko et al., Recovery improvement for large-area tungsten diselenide gas sensors. *ACS Appl. Mater. Interfaces* **10**(28), 23910–23917 (2018). <https://doi.org/10.1021/acsami.8b07034>
109. A. Moumen et al., Robust room-temperature NO₂ sensors from exfoliated 2D few-layered CVD-grown bulk tungsten diselenide (2H-WSe₂). *ACS Appl. Mater. Interfaces* **13**(3), 4316–4329 (2021). <https://doi.org/10.1021/acsami.0c17924>
110. C. Anichini, W. Czepa, D. Pakulski, A. Aliprandi, A. Ciesielski, P. Samorì, Chemical sensing with 2D materials. *Chem. Soc. Rev.* **47**(13), 4860–4908 (2018). <https://doi.org/10.1039/c8cs00417j>
111. F.R. Simões, M.G. Xavier, 6—*electrochemical sensors* (Elsevier Inc., 2017)
112. H.L. Chia, C.C. Mayorga-Martinez, M. Pumera, Doping and decorating 2D materials for biosensing: benefits and drawbacks. *Adv. Funct. Mater.* **31**(46), 1–31 (2021). <https://doi.org/10.1002/adfm.202102555>
113. T. Yang et al., A review of ratiometric electrochemical sensors: From design schemes to future prospects. *Sens. Actuators, B Chem.* **274**, 501–516 (2018). <https://doi.org/10.1016/j.snb.2018.07.138>
114. R.E. Munteanu, P.S. Moreno, M. Bramini, G. Gáspár, 2D materials in electrochemical sensors for in vitro or in vivo use. *Anal. Bioanal. Chem.* (2020). <https://doi.org/10.1007/s00216-020-02831-1>
115. R. Zribi, G. Neri, Mo-based layered nanostructures for the electrochemical sensing of biomolecules. *Sensors (Switzerland)* **20**(18), 1–23 (2020). <https://doi.org/10.3390/s20185404>
116. M.Z. Mohamad Nasir, M. Pumera, Emerging mono-elemental 2D nanomaterials for electrochemical sensing applications: from borophene to bismuthene. *TrAC Trends Anal. Chem.* **121**, 1–9 (2019). <https://doi.org/10.1016/j.trac.2019.115696>
117. M.T. Rahman et al., Graphene oxide-silver nanowire nanocomposites for enhanced sensing of Hg²⁺. *ACS Appl. Nano Mater.* **2**(8), 4842–4851 (2019). <https://doi.org/10.1021/acsanm.9b00789>
118. S.M. Choi, D.M. Kim, O.S. Jung, Y.B. Shim, A disposable chronocoulometric sensor for heavy metal ions using a diaminoterthiophene-modified electrode doped with graphene oxide. *Anal. Chim. Acta* **892**, 77–84 (2015). <https://doi.org/10.1016/j.jca.2015.08.037>
119. C. Outline, “Electrochemical techniques for environmental analysis,” (2020). <https://doi.org/10.1016/B978-0-12-816934-6.00008-4>
120. V. Dhinakaran, K. Vigneswari, M. Lavanya, and M. V. Shree, *Point-of-care applications with graphene in human life*, 1st ed., 91. Elsevier B.V., (2020)
121. N. Murugan, R. Jerome, M. Preethika, A. Sundaramurthy, A.K. Sundramoorthy, 2D-titanium carbide (MXene) based selective electrochemical sensor for simultaneous detection of ascorbic acid, dopamine and uric acid. *J. Mater. Sci. Technol.* **72**, 122–131 (2021). <https://doi.org/10.1016/j.jmst.2020.07.037>
122. J.S. Ribeiro, M.B.J.G. Freitas, J.C.C. Freitas, Recycling of graphite and metals from spent Li-ion batteries aiming the production of graphene/CoO-based electrochemical sensors. *J. Environ. Chem. Eng.* **9**(1), 104689 (2021). <https://doi.org/10.1016/j.jece.2020.104689>
123. X. Chen, X. Tian, L. Zhao, Nonenzymatic sensing of glucose at neutral pH values using a glassy carbon electrode modified with graphene nanosheets and Pt-Pd bimetallic nanocubes. *Microchim. Acta.* (2014). <https://doi.org/10.1007/s00604-013-1142-0>
124. F. Foroughi, M. Rahsepar, M.J. Hadianfard, H. Kim, Microwave-assisted synthesis of graphene modified CuO nanoparticles for voltammetric enzyme-free sensing of glucose at biological pH values. *Microchim. Acta.* **185**, 1–9 (2018)
125. M. Wang et al., A novel H₂O₂ electrochemical sensor based on NiCo₂S₄ functionalized reduced graphene oxide. *J. Alloys Compd.* (2019). <https://doi.org/10.1016/j.jallcom.2019.01.043>
126. T. Hang et al., Hierarchical graphene/nanorods-based H₂O₂ electrochemical sensor with self-cleaning and anti-biofouling properties. *Sens.*

- Actuators B. Chem. **289**, 15–23 (2019). <https://doi.org/10.1016/j.snb.2019.03.038>
127. S.A. Bhat et al., Self-assembled AuNPs on sulphur-doped graphene: a dual and highly efficient electrochemical sensor for nitrite (NO₂⁻) and nitric oxide (NO). *New J. Chem.* **41**, 8347–8358 (2017). <https://doi.org/10.1039/c7nj01565h>
128. Y. Wei et al., “SnO₂/reduced graphene oxide nanocomposite for the simultaneous electrochemical detection of cadmium (II), Lead (II), Copper (II), and mercury (II): an interesting favorable mutual interference,” 1034–1041, (2012)
129. A. Neog, R. Biswas, WS₂ nanosheets as a potential candidate towards sensing heavy metal ions: a new dimension of 2D materials. *Mater. Res. Bull.* **144**, 111471 (2021). <https://doi.org/10.1016/j.materresbull.2021.111471>
130. V. Pifferi, A. Testolin, C. Ingrosso, M.L. Curri, I. Palchetti, L. Falciola, Au nanoparticles decorated graphene-based hybrid nanocomposite for As(III) electroanalytical detection. *Chemosensors* **10**, 2 (2022). <https://doi.org/10.3390/chemosensors10020067>
131. Z. Sun, Q. Xiao, J. Tang, Y. Wang, Ratiometric electrochemical sensor for bisphenol A detection using a glassy carbon electrode modified with a poly (toluidine blue) / gold nanoparticle. *Anal. Methods* (2021). <https://doi.org/10.1039/d1ay01366a>
132. Z. Chen, C. Liu, X. Su, W. Zhang, X. Zou, Signal on-off ratiometric electrochemical sensor based on semi-complementary aptamer couple for sensitive cadmium detection in mussel. *Sens. Actuators B. Chem.* **346**, 130506 (2021). <https://doi.org/10.1016/j.snb.2021.130506>
133. Y. Xu, X. Wang, C. Ding, X. Luo, Ratiometric antifouling electrochemical biosensors based on multifunctional peptides and MXene loaded with au nanoparticles and methylene blue. *ACS Appl. Mater. Interfaces* (2021). <https://doi.org/10.1021/acsami.1c04933>
134. Z. Qu et al., Tailoring oxygen-containing groups on graphene for ratiometric electrochemical measurements of ascorbic acid in living subacute Parkinson's disease mouse brains. *Anal. Chem.* (2021). <https://doi.org/10.1021/acs.analchem.1c03965>
135. X. Wang et al., A facile ratiometric electrochemical strategy for ultrasensitive monitoring HER2 using polydopamine-grafted-ferrocene / reduced graphene oxide, Au @ Ag nanoshuttles and hollow Ni @ PtNi yolk-shell nanocages. *Sens. Actuators B. Chem.* **331**, 129460 (2021). <https://doi.org/10.1016/j.snb.2021.129460>
136. W. Zhong et al., MXene @ Ag-based ratiometric electrochemical sensing strategy for effective detection of carbendazim in vegetable samples. *Food Chem.* **360**, 130006 (2021). <https://doi.org/10.1016/j.foodchem.2021.130006>
137. N.F. Santos et al., IR and UV laser-induced graphene application as dopamine electrochemical sensors. *Adv. Mater. Technol.* **6**(6), 2100007 (2021). <https://doi.org/10.1002/admt.202100007>
138. X. Fang et al., Nanocomposites of Zr(IV)-based Metal-organic frameworks and reduced graphene oxide for electrochemically sensing ciprofloxacin in water. *ACS Appl. Nano Mater.* **2**(4), 2367–2376 (2019). <https://doi.org/10.1021/acsanm.9b00243>
139. A. Scandurra, F. Ruffino, M. Urso, M.G. Grimaldi, S. Mirabella, Disposable and low-cost electrode based on graphene paper-*nafion*-bi nanostructures for ultra-trace determination of pb(II) and cd(II). *Nanomaterials* **10**(8), 1–16 (2020). <https://doi.org/10.3390/nano10081620>
140. J. Pizarro, R. Segura, D. Tapia, F. Navarro, F. Fuenzalida, M. Jesús Aguirre, Inexpensive and green electrochemical sensor for the determination of Cd(II) and Pb(II) by square wave anodic stripping voltammetry in bivalve mollusks. *Food Chem.* (2020). <https://doi.org/10.1016/j.foodchem.2020.126682>
141. S. Deshmukh et al., Red mud-reduced graphene oxide nanocomposites for the electrochemical sensing of arsenic. *ACS Appl. Nano Mater.* **3**(5), 4084–4090 (2020). <https://doi.org/10.1021/acsanm.0c00165>
142. G. Bahuguna, M. Verma, R. Gupta, Chemical insights into electrophilic fluorination of SnO₂ for photoelectrochemical applications. *J. Mater. Chem. A* **9**(35), 19965–19974 (2021). <https://doi.org/10.1039/D1TA02560K>
143. V. Shukla, J. Wörnã, N.K. Jena, A. Grigoriev, R. Ahuja, Toward the realization of 2D borophene based gas sensor. *J. Phys. Chem. C* **121**(48), 26869–26876 (2017). <https://doi.org/10.1021/acs.jpcc.7b09552>
144. A. Shahbazi Kootenaei, G. Ansari, B36 borophene as an electronic sensor for formaldehyde: quantum chemical analysis. *Phys. Lett. Sect. A Gen. At. Solid State Phys.* **380**(34), 2664–2668 (2016). <https://doi.org/10.1016/j.physleta.2016.06.016>
145. A. Omidvar, Borophene: a novel boron sheet with a hexagonal vacancy offering high sensitivity for hydrogen cyanide detection. *Comput. Theor. Chem.* **1115**, 179–184 (2017). <https://doi.org/10.1016/j.comptc.2017.06.018>
146. S. Güngör, C. Taşaltın, İ Gürol, G. Baytemir, S. Karakuş, N. Taşaltın, Copper phthalocyanine-borophene nanocomposite-based non-enzymatic electrochemical urea biosensor. *Appl. Phys. A Mater. Sci. Process.* **128**, 1 (2022). <https://doi.org/10.1007/s00339-021-05228-8>
147. C. Taşaltın, Glucose sensing performance of PAN: β-rhombohedral borophene based non-enzymatic electrochemical biosensor. *Inorg. Chem. Commun.* (2021). <https://doi.org/10.1016/j.inoche.2021.108973>
148. A.O. Idris, E.O. Oseghe, T.A.M. Msagati, A.T. Kuvarega, U. Feleni, B. Mamba, Graphitic carbon nitride: a highly electroactive nanomaterial for environmental and clinical sensing. *Sensors (Switzerland)* **20**, 1–28 (2020). <https://doi.org/10.3390/s20205743>
149. X. Chen et al., A green method to synthesize AuNPs/mpg-C₃N₄ nanocomposites for constructing anti-interference electrochemical sensing interface toward methylmercury. *J. Alloys Compd.* (2021). <https://doi.org/10.1016/j.jallcom.2020.157365>
150. T. Kokulnathan, E.A. Kumar, T.J. Wang, Design and in situ synthesis of titanium carbide/boron nitride nanocomposite: investigation of electrocatalytic activity for the sulfadiazine sensor. *ACS Sustain. Chem. Eng.* **8**(33), 12471–12481 (2020). <https://doi.org/10.1021/acsschemeng.0c03281>
151. S. Chen et al., Direct growth of polycrystalline GaN porous layer with rich nitrogen vacancies: application to catalyst-free electrochemical detection. *ACS Appl. Mater. Interfaces* **12**(48), 53807–53815 (2020). <https://doi.org/10.1021/acsami.0c15824>
152. Q. Liu et al., Simultaneous detection of trace Ag(I) and Cu(II) ions using homeopitaxially grown GaN micropillar electrode. *Anal. Chim. Acta* **1100**, 22–30 (2020). <https://doi.org/10.1016/j.aca.2019.11.010>
153. Y. Yi, Y. Ma, F. Ai, Y. Xia, H. Lin, G. Zhu, Novel methodology for anodic stripping voltammetric sensing of heavy-metal ions using Ti₃C₂T_x nanoribbons. *Chem. Commun.* **57**(63), 7790–7793 (2021). <https://doi.org/10.1039/d1cc02560k>
154. W. Xu et al., Electrochemical biosensor based on HRP/Ti₃C₂/Nafion film for determination of hydrogen peroxide in serum samples of patients with acute myocardial infarction. *ACS Biomater. Sci. Eng.* **7**(6), 2767–2773 (2021). <https://doi.org/10.1021/acsbomaterials.1c00242>
155. S. Gul et al., Un-doped and Er-adsorbed layered Nb₂C MXene for efficient hydrazine sensing application. *Surfaces Interfaces* **24**, 101074 (2021). <https://doi.org/10.1016/j.surfint.2021.101074>
156. P.A. Rasheed, R.P. Pandey, K.A. Jabbar, J. Ponraj, K.A. Mahmoud, Sensitive electrochemical detection of L-cysteine based on a highly stable Pd@Ti₃C₂T_x(MXene) nanocomposite modified glassy carbon electrode. *Anal. Methods* **11**(30), 3851–3856 (2019). <https://doi.org/10.1039/c9ay00912d>
157. J.H. Hwang et al., Improving electrochemical Pb²⁺ detection using a vertically aligned 2D MoS₂ nanofilm. *Anal. Chem.* **91**(18), 11770–11777 (2019). <https://doi.org/10.1021/acs.analchem.9b02382>
158. C.S. Lee, T.H. Kim, Large-scale preparation of MoS₂/graphene composites for electrochemical detection of Morin. *ACS Appl. Nano Mater.* **4**(7), 6668–6677 (2021). <https://doi.org/10.1021/acsanm.1c00622>
159. J. Yuan, L. Jiang, J. Che, G. He, H. Chen, Composites of NiS₂ microblocks, MoS₂ nanosheets, and reduced graphene oxide for energy storage and electrochemical detection of bisphenol A. *ACS Appl. Nano Mater.* **4**(6), 6093–6102 (2021). <https://doi.org/10.1021/acsanm.1c00908>
160. W.Y. Zhou, S.S. Li, X.Y. Xiao, S.H. Chen, J.H. Liu, X.J. Huang, Defect- and phase-engineering of Mn-mediated MoS₂ nanosheets for ultrahigh electrochemical sensing of heavy metal ions: chemical interaction-driven in situ catalytic redox reactions. *Chem. Commun.* **54**(67), 9329–9332 (2018). <https://doi.org/10.1039/c8cc04575e>
161. H. Yuan et al., Hierarchical core-shell structure of 2D VS₂@VC@N-doped carbon sheets decorated by ultrafine Pd nanoparticles: assembled in a 3D rosette-like array on carbon fiber microelectrode for electrochemical sensing. *ACS Appl. Mater. Interfaces* **12**(13), 15507–15516 (2020). <https://doi.org/10.1021/acsami.9b21436>

162. K.R.G. Lim et al., 2H-MoS₂ on Mo₂CT_x MXene nanohybrid for efficient and durable electrocatalytic hydrogen evolution. *ACS Nano* **14**(11), 16140–16155 (2020). <https://doi.org/10.1021/acsnano.0c08671>
163. Y. Su, D. Liu, G. Yang, L. Wang, J.M. Razal, W. Lei, Light-controlled ionic transport through molybdenum disulfide membranes. *ACS Appl. Mater. Interfaces* **13**(29), 34679–34685 (2021). <https://doi.org/10.1021/acsmi.1c04698>
164. Z. Lv et al., Co-Constructing interfaces of multiheterostructure on MXene (Ti₃C₂T_x)-modified 3D self-supporting electrode for ultraefficient electrocatalytic HER in Alkaline media. *Adv. Funct. Mater.* **31**(29), 1–8 (2021). <https://doi.org/10.1002/adfm.202102576>
165. H. Xu et al., Fabrication of layered double hydroxide microcapsules mediated by cerium doping in metal-organic frameworks for boosting water splitting. *Energy Environ. Sci.* **13**(9), 2949–2956 (2020). <https://doi.org/10.1039/d0ee02113j>
166. X. Zhao, G. Hu, G.F. Chen, H. Zhang, S. Zhang, H. Wang, Comprehensive understanding of the thriving ambient electrochemical nitrogen reduction reaction. *Adv. Mater.* **33**(33), 1–46 (2021). <https://doi.org/10.1002/adma.202007650>
167. D. Liu et al., Development of electrocatalysts for efficient nitrogen reduction reaction under ambient condition. *Adv. Funct. Mater.* **31**(11), 1–36 (2021). <https://doi.org/10.1002/adfm.202008983>
168. G. Zhang, Y. Li, C. He, X. Ren, P. Zhang, H. Mi, Recent progress in 2D catalysts for photocatalytic and electrocatalytic artificial nitrogen reduction to ammonia. *Adv. Energy Mater.* **11**(11), 1–21 (2021). <https://doi.org/10.1002/aenm.202003294>
169. L. Zhang et al., A janus Fe-SnO₂ catalyst that enables bifunctional electrochemical nitrogen fixation. *Angew. Chemie* **132**(27), 10980–10985 (2020). <https://doi.org/10.1002/ange.202003518>
170. Y. Guo et al., Highly efficient electrochemical reduction of nitrogen to ammonia on surface termination modified Ti₃C₂T_xMXene nanosheets. *ACS Nano* **14**(7), 9089–9097 (2020). <https://doi.org/10.1021/acsnano.0c04284>
171. G. Peng, J. Wu, M. Wang, J. Niklas, H. Zhou, C. Liu, Nitrogen-defective polymeric carbon nitride nanolayer enabled efficient electrocatalytic nitrogen reduction with high faradaic efficiency. *Nano Lett.* **20**(4), 2879–2885 (2020). <https://doi.org/10.1021/acsnanolett.0c00698>
172. Y.M. Jo, K. Lim, H.J. Choi, J.W. Yoon, S.Y. Kim, J.H. Lee, 2D metal-organic framework derived co-loading of Co₃O₄ and PdO nanocatalysts on In₂O₃ hollow spheres for tailored design of high-performance breath acetone sensors. *Sens. Actuators B Chem.* (2020). <https://doi.org/10.1016/j.snb.2020.128821>
173. T. Yuan et al., Two-dimensional amorphous SnOx from liquid metal: mass production, phase transfer, and electrocatalytic CO₂ reduction toward formic acid. *Nano Lett.* **20**(4), 2916–2922 (2020). <https://doi.org/10.1021/acsnanolett.0c00844>
174. M.T. Nguyen et al., Synergistic effect of the oleic acid and oleylamine mixed-liquid matrix on particle size and stability of sputtered metal nanoparticles. *ACS Sustain. Chem. Eng.* **8**(49), 18167–18176 (2020). <https://doi.org/10.1021/acssuschemeng.0c06549>
175. J. Lao, R. Lv, J. Gao, A. Wang, J. Wu, J. Luo, Aqueous stable Ti₃C₂ MXene membrane with fast and photoswitchable nanofluidic transport. *ACS Nano* **12**(12), 12464–12471 (2018). <https://doi.org/10.1021/acsnano.8b06708>
176. D. Stein, M. Kruithof, C. Dekker, Surface-charge-governed ion transport in nanofluidic channels. *Phys. Rev. Lett.* **93**, 3 (2004). <https://doi.org/10.1103/PhysRevLett.93.035901>
177. K.G. Zhou et al., Electrically controlled water permeation through graphene oxide membranes. *Nature* **559**(7713), 236–240 (2018). <https://doi.org/10.1038/s41586-018-0292-y>
178. C. Cheng, G. Jiang, G.P. Simon, J.Z. Liu, D. Li, Low-voltage electrostatic modulation of ion diffusion through layered 2 graphene-based nanoporous membranes. *Nat Nanotech* (2018). <https://doi.org/10.1038/s41565-018-0181-4>
179. T. Liang, J. Hou, J. Xi, Mechanisms of nanofluid based modification MoS₂ nanosheet for enhanced oil recovery in terms of interfacial tension, wettability alteration and emulsion stability. *J. Dispers. Sci. Technol.* (2021). <https://doi.org/10.1080/01932691.2021.1930034>
180. Y. Feng, L. Ding, D. Ji, L. Wang, W. Guo, Highly rectified ion transport through 2D WSe₂/MoS₂ bi-layered membranes. *Chin. Chem. Lett.* **29**(6), 892–894 (2018). <https://doi.org/10.1016/j.ccl.2018.01.053>
181. W. Lei, V.N. Mochalin, D. Liu, S. Qin, Y. Gogotsi, Y. Chen, Boron nitride colloidal solutions, ultralight aerogels and freestanding membranes through one-step exfoliation and functionalization. *Nat. Commun.* (2015). <https://doi.org/10.1038/ncomms9849>
182. S. Qin et al., High and stable ionic conductivity in 2D nanofluidic ion channels between boron nitride layers. *J. Am. Chem. Soc.* **139**(18), 6314–6320 (2017). <https://doi.org/10.1021/jacs.6b11100>
183. M. Abdollahzadeh et al., Low humid transport of anions in layered double hydroxides membranes using polydopamine coating. *J. Memb. Sci.* (2021). <https://doi.org/10.1016/j.memsci.2020.118974>
184. Y. Xie, Y. Zheng, J. Fan, Y. Wang, L. Yue, N. Zhang, Novel electronic-ionic hybrid conductive composites for multifunctional flexible bioelectrode based on in situ synthesis of poly(dopamine) on bacterial cellulose. *ACS Appl. Mater. Interfaces* **10**(26), 22692–22702 (2018). <https://doi.org/10.1021/acsmi.8b05345>
185. Z. Sun et al., Highly ionic conductive and mechanically strong MXene/CNF membranes for osmotic energy conversion. *Sustain. Energy Fuels* **6**(2), 299–308 (2022). <https://doi.org/10.1039/d1se01729b>
186. M. Liu, P.J. Weston, R.H. Hurt, Controlling nanochannel orientation and dimensions in graphene-based nanofluidic membranes. *Nat. Commun.* **12**(1), 1–7 (2021). <https://doi.org/10.1038/s41467-020-20837-2>
187. Z. He, R. Zhou, Exploring an in-plane graphene and hexagonal boron nitride array for separation of single nucleotides. *ACS Nano* **15**(7), 11704–11710 (2021). <https://doi.org/10.1021/acsnano.1c02450>
188. J. Park et al., Unusually high ion conductivity in large-scale patternable two-dimensional MoS₂ film. *ACS Nano* **15**(7), 12267–12275 (2021). <https://doi.org/10.1021/acsnano.1c04054>
189. N. Zhan, M. Olmedo, G. Wang, J. Liu, Graphene based nickel nanocrystal flash memory. *Appl Phys Lett* **99**, 113112 (2011). <https://doi.org/10.1063/1.3640210>
190. J.J. Yang, D.B. Strukov, D.R. Stewart, Memristive devices for computing. *Nat Nanotechnol.* **8**, 13–24 (2013). <https://doi.org/10.1038/nnano.2012.240>
191. A. Gurarlan, S. Jiao, T.D. Li, Van der Waals force isolation of monolayer MoS₂. *Adv. Mater.* **28**, 10055–10060 (2016). <https://doi.org/10.1002/adma.20160158>
192. E. Zhang, W. Wang, C. Zhang, Tunable charge-trap memory based on few-layer MoS₂. *ACS Nano* **9**, 612–619 (2014). <https://doi.org/10.1021/nn5059419>
193. D. Li, X. Wang, Q. Zhang, L. Zou, X. Xu, Z. Zhang, Nonvolatile floating-gate memories based on stacked black phosphorus–boron nitride–MoS₂ heterostructures. *Adv. Funct. Mater.* **25**, 7360–7365 (2015). <https://doi.org/10.1002/adfm.201503645>
194. Q. Feng, F. Yan, W. Luo, K. Wang, Charge trap memory based on few-layer black phosphorus. *Nanoscale* **8**, 2686–2692 (2016). <https://doi.org/10.1039/C5NR08065G>
195. C. Liu, X. Yan, X. Song, S. Ding, D.W. Zhang, P. Zhou, A semifloating gate memory based on van der Waals heterostructures for quasi-non-volatile applications. *Nat Nanotechnol.* **13**, 404–410 (2018). <https://doi.org/10.1038/s41565-018-0102-6>
196. J. Li, L. Liu, X. Chen et al., Symmetric ultrafast writing and erasing speeds in quasi-nonvolatile memory via van der Waals heterostructures. *Adv. Mater.* (2019). <https://doi.org/10.1002/adma.201808035>
197. R. Buyya, C.S. Yeo, S. Venugopal, J. Broberg, I. Brandic, Cloud computing and emerging IT platforms: vision, hype, and reality for delivering computing as the 5th utility. *Future Gener. Comput. Syst.* **25**, 599–616 (2009). <https://doi.org/10.1016/j.future.2008.12.001>
198. G. Meijer, Who wins the nonvolatile memory race? *Science* **319**, 1625–1626 (2008). <https://doi.org/10.1126/science.1153909>
199. A.C. Neto, F. Guinea, N.M. Peres, K.S. Novoselov, A.K. Geim, The electronic properties of graphene. *Rev Mod Phys.* **81**, 109–162 (2009). <https://doi.org/10.1103/RevModPhys.81.109>
200. C.R. Dean, A.F. Young, I. Meric et al., Boron nitride substrates for high-quality graphene electronics. *Nat Nanotechnol.* **5**, 722–726 (2010). <https://doi.org/10.1038/nnano.2010.172>

201. Q.H. Wang, K. Kalantarzadeh, A. Kis, J.N. Coleman, M.S. Strano, Electronics and optoelectronics of two-dimensional transition metal dichalcogenides. *Nat Nanotechnol.* **7**, 699–712 (2012). <https://doi.org/10.1038/nnano.2012.193>
202. X. Cui, G.H. Lee, Y.D. Kim et al., Multi-terminal transport measurements of MoS₂ using a van der Waals heterostructure device platform. *Nat Nanotechnol* **10**, 534–540 (2015). <https://doi.org/10.1038/nnano.2015.70>
203. Y. Liu, N.O. Weiss, X. Duan, H.C. Cheng, Y. Huang, X. Duan, Van der Waals heterostructures and devices. *Nat Rev Mater.* **1**, 16042 (2016). <https://doi.org/10.1038/natrevmats.2016.42>
204. Q.A. Vu, Y.S. Shin, Y.R. Kim et al., Two-terminal floating-gate memory with van der Waals heterostructures for ultrahigh on/off ratio. *Nat Commun.* **7**, 12725 (2016). <https://doi.org/10.1038/ncomms12725>
205. Q.A. Vu, H. Kim, V.L. Nguyen, U.Y. Won, S. Adhikari, K. Kim, Y.H. Lee, W.J. Yu, A high-on/off-ratio floating-gate Memristor array on a flexible substrate via CVD-grown large-area 2D layer stacking. *Adv. Mater.* **29**, 1703363 (2017). <https://doi.org/10.1002/adma.201703363>
206. S. Choi, M. Lee, G.H. Yu, Y.J. Yu et al., Controlled charge trapping by molybdenum disulphide and graphene in ultrathin heterostructured memory devices. *Nat Commun* **4**, 1624 (2013). <https://doi.org/10.1038/ncomms2652>
207. S. Bertolazzi, P. Bondavalli, S. Roche, T. San, S.Y. Choi, L. Colombo, F. Bonaccorso, P. Samori, Nonvolatile memories based on graphene and related 2D materials. *Adv Mater.* (2019). <https://doi.org/10.1002/adma.201806663>
208. Y. Li, A. Sinitskii, J. Tour, Electronic two-terminal bistable graphitic memories. *Nature Mater* **7**, 966–971 (2008). <https://doi.org/10.1038/nmat2331>
209. B. Standley, W. Bao, H. Zhang, J. Bruck, C.N. Lau, M. Bockrath, Graphene-based atomic-scale switches. *Nano Lett.* **8**, 3345 (2008). <https://doi.org/10.1021/nl801774a>
210. A. Sinitskii, J.M. Tour, Lithographic graphitic memories. *ACS Nano* **3**, 2760 (2009). <https://doi.org/10.1021/nn9006225>
211. C.L. He, F. Zhuge, X.F. Zhou, M. Li, G.C. Zhou, Y.W. Liu, J.Z. Wang, B. Chen, W.J. Su, Z.P. Liu, Y.H. Wu, P. Cui, R.-W. Li, Nonvolatile resistive switching in graphene oxide thin films. *Appl. Phys. Lett.* **95**, 232101 (2009). <https://doi.org/10.1063/1.3271177>
212. H.Y. Jeong, J.Y. Kim, J.W. Kim, J.O. Hwang, J.-E. Kim, J.Y. Lee, T.H. Yoon, B.J. Cho, S.O. Kim, R.S. Ruoff, S.-Y. Choi, Graphene oxide thin films for flexible nonvolatile memory applications. *Nano Lett.* **10**, 4381 (2010). <https://doi.org/10.1021/nl101902k>
213. S.K. Hong, J.E. Kim, S.O. Kim, S.Y. Choi, B.J. Cho, Flexible resistive switching memory device based on graphene oxide. *IEEE Electron Device Lett.* **31**, 1005 (2010). <https://doi.org/10.1109/LED.2010.2053695>
214. G.N. Panin, O.O. Kapitanova, S.W. Lee, A.N. Baranov, T.W. Kang, Resistive switching in Al/graphene oxide/Al structure. *Jpn. J. Appl. Phys.* **50**, 070110 (2011). <https://doi.org/10.1143/JJAP.50.070110>
215. K.S. Vasu, S. Sampath, A.K. Sood, Nonvolatile unipolar resistive switching in ultrathin films of graphene and carbon nanotubes. *Solid State Commun.* **151**, 1084 (2011). <https://doi.org/10.1016/j.ssc.2011.05.018>
216. C.X. Wu, F.S. Li, Y.G. Zhang, T.L. Guo, Recoverable electrical transition in a single graphene sheet for application in nonvolatile memories. *Appl. Phys. Lett.* **100**, 042105 (2012). <https://doi.org/10.1063/1.3680093>
217. C. Jin, J. Lee, E. Lee, E. Hwang, H. Lee, Nonvolatile resistive memory of ferrocene covalently bonded to reduced graphene oxide. *Chem. Commun.* **48**, 4235 (2012). <https://doi.org/10.1039/C2CC30973D>
218. P. Cui, S. Seo, J. Lee, L. Wang, E. Lee, M. Min, H. Lee, Nonvolatile memory device using gold nanoparticles covalently bound to reduced graphene oxide. *ACS Nano* **5**, 6826 (2011). <https://doi.org/10.1021/nn2021875>
219. J. Liu, Z. Zeng, X. Cao, G. Lu, L.-H. Wang, Q.-L. Fan, W. Huang, H. Zhang, Preparation of MoS₂-polyvinylpyrrolidone nanocomposites for flexible nonvolatile rewritable memory devices with reduced graphene oxide electrodes. *Small* **8**, 3517 (2012). <https://doi.org/10.1002/sml.201200999>
220. X. Hong, J. Liu, B. Zheng, X. Huang, X. Zhang, C. Tan, J. Chen, Z. Fan, H. Zhang, A universal method for preparation of noble metal nanoparticle-decorated transition metal dichalcogenide nanobelts. *Adv. Mater.* **26**, 6250 (2014). <https://doi.org/10.1002/adma.201402063>
221. Z. Yin, Z. Zeng, J. Liu, Q. He, P. Chen, H. Zhang, Memory devices using a mixture of MoS₂ and graphene oxide as the active layer. *Small* **9**, 727 (2013). <https://doi.org/10.1002/sml.201201940>
222. G.H. Shin, C.-K. Kim, G.S. Bang, J.Y. Kim, B.C. Jang, B.J. Koo, M.H. Woo, Y.-K. Choi, S.-Y. Choi, Multilevel resistive switching nonvolatile memory based on MoS₂ nanosheet-embedded graphene oxide. *2D Mater.* **3**, 034002 (2016). <https://doi.org/10.1088/2053-1583/3/3/034002>
223. S. Bhattacharjee, P.K. Sarkar, M. Prajapat, A. Roy, Flexible, transparent resistive switching device based on topological insulator Bi₂Se₃-organic composite. *J. Phys. D: Appl. Phys.* **50**, 265103 (2017). <https://doi.org/10.1063/1.5042332>
224. M.M. Rehman, G.U. Siddiqui, J.Z. Gul, S.-W. Kim, J.H. Lim, K.H. Choi, Resistive switching in all-printed, flexible and hybrid MoS₂-PVA nanocomposite based memristive device fabricated by reverse offset. *Sci. Rep.* **6**, 36195 (2016). <https://doi.org/10.1038/srep36195>
225. A.A. Bessonov, M.N. Kirikova, D.I. Petukhov, M. Allen, T. Ryhänen, M.J.A. Bailey, Layered memristive and memcapacitive switches for printable electronics. *Nat. Mater.* (2015). <https://doi.org/10.1038/nmat4135>
226. P.F. Cheng, K. Sun, Y.H. Hu, Memristive behavior and ideal memristor of 1T phase MoS₂ nanosheets. *Nano Lett.* **16**, 572 (2016). <https://doi.org/10.1021/acs.nanolett.5b04260>
227. V.K. Sangwan, D. Jariwala, I.S. Kim, K.-S. Chen, T.J. Marks, L.J. Lauhon, M.C. Hersam, Gate-tunable memristive phenomena mediated by grain boundaries in single-layer MoS₂. *Nat. Nanotechnol.* **10**, 403 (2015). <https://doi.org/10.1038/nnano.2015.56>
228. K. Qian, R.Y. Tay, V.C. Nguyen, J. Wang, G. Cai, T. Chen, E.H.T. Teo, P.S. Lee, Hexagonal boron nitride thin film for flexible resistive memory applications. *Adv. Funct. Mater.* **26**, 2176 (2016). <https://doi.org/10.1002/adfm.201504771>
229. C. Pan, Y. Ji, N. Xiao, F. Hui, K. Tang, Y. Guo, X. Xie, F.M. Puglisi, L. Larcher, E. Miranda, L. Jiang, Y. Shi, I. Valov, P.C. McIntyre, R. Waser, M. Lanza, Coexistence of grain-boundaries-assisted bipolar and threshold resistive switching in multilayer hexagonal boron nitride. *Adv. Funct. Mater.* **27**, 1604811 (2017). <https://doi.org/10.1002/adfm.201604811>
230. C.X. Hao, F.S. Wen, J.Y. Xiang, S.J. Yuan, B.C. Yang, L. Li, W.H. Wang, Z.M. Zeng, L.M. Wang, Z.Y. Liu, Y.J. Tian, Liquid-exfoliated black phosphorous nanosheet thin films for flexible resistive random access memory applications. *Adv. Funct. Mater.* **26**, 12 (2016). <https://doi.org/10.1002/adfm.201504187>
231. S. Wang, J. Pu, D.S.H. Chan, B.J. Cho, K.P. Loh, Wide memory window in graphene oxide charge storage nodes. *Appl. Phys. Lett.* **96**, 143109 (2010). <https://doi.org/10.1063/1.3383234>
232. J.K. Park, S.M. Song, J.H. Mun, B.J. Cho, Graphene gate electrode for MOS structure-based electronic devices. *Nano Lett.* **11**, 5383 (2011). <https://doi.org/10.1021/nl202983x>
233. M.S. Choi, G.-H. Lee, Y.-J. Yu, D.-Y. Lee, S. Hwan Lee, P. Kim, J. Hone, W. Jong Yoo, Controlled charge trapping by molybdenum disulphide and graphene in ultrathin heterostructured memory devices. *Nat. Commun.* **4**, 1624 (2013). <https://doi.org/10.1038/ncomms2652>
234. X. Shao, A. Khurshid, A review paper on “graphene field emission for electron microscopy.” *Appl. Sci.* **8**, 868 (2018). <https://doi.org/10.3390/app8060868>
235. N. Dwivedi, C. Dhand, J.D. Carey, E.C. Anderson, R. Kumar, A.K. Srivastava, H.K. Malik, M.S.M. Saifullah, S. Kumar, R. Lakshminarayanan, S. Ramakrishna, C.S. Bhatia, A. Danner, The rise of carbon materials for field emission. *J Mater. Chem. C* **9**, 2620–2659 (2021). <https://doi.org/10.1039/D0TC05873D>
236. W.P. Dyke, W.W. Dolan, Field emission. *Adv. Electron. Electron Phys.* **8**, 89–185 (1956). [https://doi.org/10.1016/S0065-2539\(08\)61226-3](https://doi.org/10.1016/S0065-2539(08)61226-3)
237. Y.S. Ang, L. Cao, L.K. Ang, Physics of electron emission and injection in two-dimensional materials: theory and simulation. *InfoMat* (2021). <https://doi.org/10.1002/inf2.12168>
238. P. Musumeci, L. Cultrera, M. Ferrario, D. Filippetto, G. Gatti, M.S. Gutierrez, J.T. Moody, N. Moore, J.B. Rosenzweig, C.M. Scoby, G. Travish, C. Vicario, *Phys. Rev. Lett.* **104**, 084801 (2010). <https://doi.org/10.1103/PhysRevLett.104.084801>
239. M.V. Moghaddam, P. Yaghoobi, G.A. Sawatzky, A. Nojeh, Photon-impenetrable, electron-permeable: the carbon nanotube forest as a medium for multiphoton thermal-photoemission. *ACS Nano* **9**, 4064–4069 (2015). <https://doi.org/10.1021/acsnano.5b00115>

240. A. Patra, M.A. More, D.J. Late, C.S. Rout, Field emission applications of graphene analogous two dimensional materials: recent developments and future perspectives. *J. Mater. Chem. C* **9**, 11059–11078 (2021). <https://doi.org/10.1039/D1TC02054D>
241. S.R. Suryawanshi, S.N. Guin, A. Chatterjee, V. Kashid, M.A. More, D.J. Late, K. Biswas, Low frequency noise and photo-enhanced field emission from ultrathin PbBi₂Se₄ nanosheets. *J. Mater. Chem. C* **4**, 1096–1103 (2016). <https://doi.org/10.1039/C5TC02993G>
242. S.T. Nishanthi, A. Baruah, K.K. Yadav, D. Sarker, S. Ghosh, A.K. Ganguli, M.J. Jha, New low temperature environmental friendly process for the synthesis of tetragonal MoO₃ and its field emission properties. *Appl. Surface Sci.* (2019). <https://doi.org/10.1016/j.apsusc.2018.10.173>
243. M. Kumar, D.Y. Park, R. Singh, M.S. Jeong, T. Som, J. Kim, *ACS Appl. Mater. Interfaces* **11**, 35845–35852 (2019)
244. R.V. Kashid, D.J. Late, S.S. Chou, Y.-K. Huang, M. De, D.S. Joag, M.A. More, V.P. Dravid, Enhanced field-emission behavior of layered MoS₂ sheets. *Small* **9**, 2730–2734 (2013). <https://doi.org/10.1002/sml.201300002>
245. P.R. Dusane, B.R. Thombare, P.K. Bankar, G. Lole, D. Gavhane, C.V. Khedkar, B. Nagrare, A. Salunkhe, P. Kolhe, R.J. Choudhary, D.M. Phase, M.A. More, S.I. Patil, Vertically aligned ultrathin MoSe₂ nanoflakes grown on carbon cloth and its field emission behaviour. *Mater. Res. Bull.* **116**, 67–71 (2019). <https://doi.org/10.1016/j.materresbull.2019.04.015>
246. B. Yang, J. Chen, X. Wu, B. Liu, L. Liu, Y. Tang, X. Yan, Enhanced field emission performance of MXene–TiO₂ composite films. *Nanoscale* **13**, 7622–7629 (2021). <https://doi.org/10.1039/D0NR08900A>
247. C. Song, K. Yu, H. Yin, H. Fu, Z. Zhang, N. Zhang, Z. Zhu, Highly efficient field emission properties of a novel layered VS₂/ZnO nanocomposite and flexible VS₂ nanosheet. *J. Mater. Chem. C* **2**, 4196–4202 (2014). <https://doi.org/10.1039/C4TC00025K>
248. C.S. Rout, P.D. Joshi, R.V. Kashid, D.S. Joag, M.A. More, A.J. Simbeck, M. Washington, S.K. Nayak, D.J. Late, Enhanced field emission properties of doped graphene nanosheets with layered SnS₂. *Appl. Phys. Lett.* **105**, 043109 (2014). <https://doi.org/10.1063/1.4892001>
249. S. Ratha, P. Bankar, A.S. Gangan, M.A. More, D.J. Late, J.N. Behera, B. Chakraborty, C.S. Rout, VSe₂-reduced graphene oxide as efficient cathode material for field emission. *J. Phys. Chem. Solids* **128**, 384–390 (2019). <https://doi.org/10.1016/j.jpcs.2018.02.020>
250. X.D. Hong, H.R. Zheng, D. Liang, Enhanced field emission properties from plasma treated Ti3C₂T_x (MXene) emitters. *Mater. Res. Express* **7**, 115011 (2020). <https://doi.org/10.1088/2053-1591/abc9e0/meta>
251. T.A.J. Loh, Y.J. Ooi, D.H.C. Chua, WS₂ nano-petals and nano-bristles supported on carbon nanotubes for electron emission applications. *Sci. Rep.* **9**, 3672 (2019). <https://doi.org/10.1038/s41598-019-39605-4>
252. E.L. Murphy, R.H. Good, Thermionic emission field emission, and the transition region. *Phys. Rev.* **102**, 1464–1473 (1956). <https://doi.org/10.1103/PhysRev.102.1464>
253. K. Vishwakarma et al., Quantum coupled borophene based heterolayers for excitonic and molecular sensing applications. *Phys. Chem. Chem. Phys.* (2022). <https://doi.org/10.1039/D2CP01712A>
254. H. Zhang, R. Lv, Defect engineering of two-dimensional materials for efficient electrocatalysis. *J. Mater.* **4**, 95–107 (2018). <https://doi.org/10.1016/j.jmat.2018.02.006>
255. M. Tomy, A.A. Rajappan, V.M. Vimuna, X.T. Suryabai, Emergence of novel 2D materials for high-performance supercapacitor electrode applications: a brief review. *Energy Fuels* **35**, 19881–19900 (2021). <https://doi.org/10.1021/acs.energyfuels.1c02743>
256. L. Zhang, K. Khan, J. Zou, H. Zhang, Y. Li, Recent advances in emerging 2D material-based gas sensors: potential in disease diagnosis. *Adv. Mater. Interfaces* **6**, 1901329 (2019). <https://doi.org/10.1002/ADMI.201901329>
257. M. Mathew, C.S. Rout, Schottky diodes based on 2D materials for environmental gas monitoring: a review on emerging trends, recent developments and future perspectives. *J. Mater. Chem. C* **9**, 395–416 (2021). <https://doi.org/10.1039/D0TC04840b>
258. B.L. Wang, Y.F. Sun, H.Y. Ding, X. Zhao, L. Zhang, J.W. Bai, K. Liu, Bioelectronics-related 2D materials beyond graphene: fundamentals, properties, and applications. *Adv. Funct. Mater.* **30**, 2003732 (2020). <https://doi.org/10.1002/adfm.202003732>
259. G. Viskadourous, A. Zak, M. Stylianakis, E. Kymakis, R. Tenne, E. Stratakis, Enhanced field emission of WS₂ nanotubes. *Small* **10**, 2398–2403 (2014). <https://doi.org/10.1002/sml.201303340>

Publisher's Note

Springer Nature remains neutral with regard to jurisdictional claims in published maps and institutional affiliations.

Submit your manuscript to a SpringerOpen® journal and benefit from:

- Convenient online submission
- Rigorous peer review
- Open access: articles freely available online
- High visibility within the field
- Retaining the copyright to your article

Submit your next manuscript at ► [springeropen.com](https://www.springeropen.com)